Chapter 2
Continuum Mechanics

2.1 Introduction

In applications to be addressed later, we will be interested in an object's motion, as well as, its internal force distribution. The internal force distribution is described through a *stress* tensor. At the same time, a description of the motion of a body, or its *kinematics*, involves knowledge of how each material point in its interior evolves with time. The kinematics is, in turn, intimately linked to the internal and external force distributions via appropriate *constitutive* and *balance laws*.

To follow the evolution of an object, we relate its configuration at any time t to its known state at some previous time. If this previous time is a fixed reference time, say the time when the body was in its virginal state, we obtain the so-called *Lagrangian* description of the motion. On the other hand, knowing the configuration of the body at time t in terms of its arrangement an infinitesimal instant before, constitutes the *Eulerian* description of motion. We will have occasion to employ both these representations.

Similarly, the stress state can be elaborated in terms of the object's present, or its reference state, leading to the *Cauchy* stress tensor, or the *first Piola–Kirchoff* tensor, respectively. These two tensors will be related to each other by a knowledge of the body's kinematics. We will preferentially employ the Cauchy stress tensor.

Finally, the kinematical response of a body to applied forces, or, conversely, the stress distribution resulting from an imposed kinematics, are both governed by constitutive laws employed to model the mechanical behavior of the object's constituent material. We will discuss one in detail which will be employed extensively later.

In this chapter, we provide a quick summary of essential continuum mechanics. For more details we refer the reader to the excellent book by Spencer (1980). It is important to note that we will develop relevant equations in a frame $\left\{\mathscr{O}, \hat{\mathbf{e}}_i(t)\right\}$ with origin O and which rotates at angular velocity $\boldsymbol{\omega}(t)$, to which we associate the tensor $\Omega(t)$. This is motivated by our ultimate aim to investigate Solar System objects, all of which rotate. In this, our formulation is a departure from standard ones that are done with respect to a fixed inertial frame $\left\{\mathscr{I}, \hat{\mathbf{i}}_i\right\}$.

I. Sharma, *Shapes and Dynamics of Granular Minor Planets*,
Advances in Geophysical and Environmental Mechanics and Mathematics,
DOI 10.1007/978-3-319-40490-5_2

2.2 Motion in a Rotating Coordinate System

We will be employing several rotating coordinate systems while investigating the motion of Solar System bodies. For this, we will need to relate rates of change of scalar, vector and tensor quantities as seen by observers in these coordinate systems.

2.2.1 Vectors and Tensors

Consider the coordinate systems $\left\{\mathscr{O}, \hat{\mathbf{e}}_i(t)\right\}$ and $\left\{\mathscr{I}, \hat{\mathbf{i}}_i\right\}$. Time differentiation in the rotating frame $\mathscr{O}$ will be indicated by '$\cdot$', while '$\mathring{\cdot}$' will identify time derivatives in the inertial frame $\mathscr{I}$.

The rotation tensor $\mathsf{R}(t)$ relating $\mathscr{I}$ and $\mathscr{O}$ is given by adapting (1.34) suitably:

$$\mathsf{R}(t) = \left\{\hat{\mathbf{i}}_i \cdot \hat{\mathbf{e}}_j(t)\right\} \hat{\mathbf{i}}_i \otimes \hat{\mathbf{i}}_j, \tag{2.1}$$

so that, following (1.35),

$$\hat{\mathbf{e}}_i = \mathsf{R} \cdot \hat{\mathbf{i}}_i.$$

Differentiating the above in $\mathscr{I}$ yields

$$\mathring{\hat{\mathbf{e}}}_i = \mathring{\mathsf{R}} \cdot \hat{\mathbf{i}}_i = \mathring{\mathsf{R}} \cdot \mathsf{R}^T \cdot \hat{\mathbf{e}}_i,$$

where in the second equality we have employed the fact that R is an orthogonal tensor so that $\hat{\mathbf{i}}_i = \mathsf{R}^T \cdot \hat{\mathbf{e}}_i$. Now, $\mathring{\mathsf{R}} \cdot \mathsf{R}^T$ is an anti-symmetric tensor. Indeed, differentiating $\mathsf{R} \cdot \mathsf{R}^T = \mathsf{1}$, we see that

$$\mathring{\mathsf{R}} \cdot \mathsf{R}^T + \mathsf{R} \cdot \mathring{\mathsf{R}}^T = \mathsf{0}.$$

so that

$$\left(\mathring{\mathsf{R}} \cdot \mathsf{R}^T\right)^T = \mathsf{R} \cdot \mathring{\mathsf{R}}^T = -\mathring{\mathsf{R}} \cdot \mathsf{R}^T.$$

Thus, we may now define the *angular velocity tensor*

$$\Omega(t) = \mathring{\mathsf{R}}(t) \cdot \mathsf{R}^T(t), \tag{2.2}$$

with the associated angular velocity $\boldsymbol{\omega}(t)$, that measures the rate at which $\mathscr{O}$ rotates with respect to $\mathscr{I}$. This is further emphasized by rewriting $\mathring{\hat{\mathbf{e}}}_i$ computed above as

$$\mathring{\hat{\mathbf{e}}}_i = \boldsymbol{\omega} \times \hat{\mathbf{e}}_i = \Omega \cdot \hat{\mathbf{e}}_i. \tag{2.3}$$

In an analogous manner, we may describe the motion of a frame $\left\{\mathscr{P}, \hat{\mathbf{e}}'_i(t)\right\}$ that rotates with respect to $\mathscr{O}$. Indeed,

$$\mathsf{R}_P(t) = \left\{\hat{\mathbf{e}}_i(t) \cdot \hat{\mathbf{e}}'_j(t)\right\} \hat{\mathbf{e}}_i(t) \otimes \hat{\mathbf{e}}_j(t),$$

will define the rotation tensor relating $\mathscr{P}$ to $\mathscr{O}$, while

$$\Omega_P(t) = \dot{\mathsf{R}}_P \cdot \mathsf{R}_P^T,$$

is the relevant angular velocity tensor, from which the angular velocity $\boldsymbol{\omega}_P(t)$ of the frame $\mathscr{P}$ relative to $\mathscr{O}$ may be found. Finally, similar to (2.3), we will have

$$\dot{\hat{\mathbf{e}}}'_i = \boldsymbol{\omega}_P \times \hat{\mathbf{e}}'_i = \Omega_P \cdot \hat{\mathbf{e}}'_i.$$

We now compute the rates of change of fields in $\mathscr{I}$ and $\mathscr{O}$. A scalar field $c(\mathbf{x}, t)$ remains oblivious of the motion of the observer, so that c changes in the same manner in both frames, i.e.,

$$\dot{c} = \mathring{c}\,; \tag{2.4}$$

here $\mathbf{x}$ is the position vector with respect to a fixed origin. However, vector and tensor fields will change differently for differently rotating observers. Consider a vector field $\mathbf{b}(\mathbf{x}, t)$, expressed as $\mathbf{b} = b_i(\mathbf{x}, t)\hat{\mathbf{e}}_i(t)$ in $\mathscr{O}$. As $\hat{\mathbf{e}}_i$ will be seen to be fixed to an observer in $\mathscr{O}$, we have $\dot{\mathbf{b}} = \dot{b}'_i\hat{\mathbf{e}}'_i$. Differentiating with respect to time in $\mathscr{I}$, and invoking (2.3) and (2.4) leads to

$$\mathring{\mathbf{b}} = \mathring{b}'_i\hat{\mathbf{e}}'_i + b'_i\mathring{\hat{\mathbf{e}}}'_i = \dot{b}'_i\hat{\mathbf{e}}'_i + b'_i\Omega \cdot \hat{\mathbf{e}}'_i = \dot{\mathbf{b}} + \Omega \cdot \mathbf{b}. \tag{2.5}$$

We follow a similar process for a time-dependent tensor field $\mathsf{A}(\mathbf{x}, t)$. We first express A in terms of its components in $\mathscr{O}$ as $\mathsf{A} = A_{ij}(\mathbf{x}, t)\hat{\mathbf{e}}_i(t) \otimes \hat{\mathbf{e}}_j(t)$, and then differentiate it in $\mathscr{I}$ via the chain rule, to obtain

$$\mathring{\mathsf{A}} = \dot{\mathsf{A}} + \Omega \cdot \mathsf{A} - \mathsf{A} \cdot \Omega, \tag{2.6}$$

where we employed (2.3). In the special case that A is Ω, we find that

$$\dot{\Omega} = \mathring{\Omega}, \tag{2.7}$$

i.e., the rate of change of $\mathscr{O}$ is the same whether it is observed from within itself or from the fixed frame $\mathscr{I}$.

2.2.2 *Velocity and Acceleration*

We now consider the motion of a particle A. Let it be viewed in both the rotating frame $\left\{\mathscr{O}, \hat{\mathbf{e}}_i\right\}$ and the inertial frame $\left\{\mathscr{I}, \hat{\mathbf{i}}_i\right\}$. Let $\mathscr{O}$'s origin O itself move with respect to $\mathscr{I}$. Note that at any given time it is possible to select $\mathscr{I}$ so that its origin

coincides momentarily with O. Our aim is to compute formulae relating the velocity and acceleration of A as measured by inertial and rotating observers.

Consider first that O is fixed and that with respect to it the particle A is located at $\mathbf{r}_A(t)$. The velocity and acceleration observed in $\mathscr{I}$ and $\mathscr{O}$ will be different. We may relate these two measurements by utilizing ideas of Sect. 2.2.1. Setting $\mathbf{b} = \mathbf{r}_A$ in (2.5) yields

$$\mathbf{v}_A^I = \mathbf{v}_A + \boldsymbol{\omega} \times \mathbf{r}_A = \mathbf{v}_A + \Omega \cdot \mathbf{r}_A,$$

where $\mathbf{v}_A^I = \mathring{\mathbf{r}}_A$ is A's *inertial velocity*, i.e., velocity relative to $\mathscr{I}$, and $\mathbf{v}_A = \dot{\mathbf{r}}_A$ is the velocity measured in the rotating frame $\mathscr{O}$. We will employ the superscript 'I' to indicate inertial measurements. To relate accelerations, we differentiate the above in $\mathscr{I}$, employ (2.7), and eliminate $\mathring{\mathbf{v}}_A$ and $\mathring{\mathbf{r}}_A$ via (2.5) to find

$$\mathbf{a}_A^I = \mathbf{a}_A + \boldsymbol{\omega} \times (\boldsymbol{\omega} \times \mathbf{r}_A) + \dot{\boldsymbol{\omega}} \times \mathbf{r}_A + 2\boldsymbol{\omega} \times \mathbf{v}_A = \mathbf{a}_A + \Omega^2 \cdot \mathbf{r}_A + \dot{\Omega} \cdot \mathbf{r}_A + 2\Omega \cdot \mathbf{v}_A,$$

where $\mathbf{a}_A^I = \mathring{\mathbf{v}}_A^I$ and $\mathbf{a}_A = \dot{\mathbf{v}}_A$ are, respectively, A's *inertial acceleration* and its acceleration relative to $\mathscr{O}$. Note that in the above we have employed (1.18) repeatedly.

When the origin O moves with inertial velocity $\mathbf{v}_O^I$ and inertial acceleration $\mathbf{a}_O^I$, the previous formulae are augmented appropriately:

$$\mathbf{v}_A^I = \mathbf{v}_O^I + \mathbf{v}_A + \Omega \cdot \mathbf{r}_A \tag{2.8a}$$

and

$$\mathbf{a}_A^I = \mathbf{a}_O^I + \mathbf{a}_A + \Omega^2 \cdot \mathbf{r}_A + \dot{\Omega} \cdot \mathbf{r}_A + 2\Omega \cdot \mathbf{v}_A. \tag{2.8b}$$

The acceleration equation above is the well-known "five-term acceleration" formula; see, e.g., Greenwood (1988, p. 50). The third term is the centripetal acceleration, the fourth is the contribution of $\mathscr{O}$'s angular acceleration, and the last is *Coriolis' acceleration* that is the difference between measuring change in relative velocity in a rotating frame compared to its evaluation in a non-rotating one.

We move on to describing the motion of a continuous body.

2.3 Kinematics

We now consider the motion of a continuous body as observed in a translating and rotating frame $\mathscr{O}$. Figure 2.1 shows the *reference* configuration of the body at some fixed time that may taken to be zero, and also the body's *current* configuration at the present time t. The reference configuration appears fixed in $\mathscr{O}$ at all times. This implies that the reference configuration translates and rotates along with $\mathscr{O}$. We will see that this does not affect the deformation of the body, and only introduces a superimposed rigid body motion.

In Fig. 2.1, we indicate the positions $\mathbf{X}_A$ and $\mathbf{x}_A(t)$ of a material point A relative to a reference point P fixed to the body, in the reference and current configurations, respectively. The vector $\mathbf{r}_P(t)$ follows the motion of P with respect to the origin O of

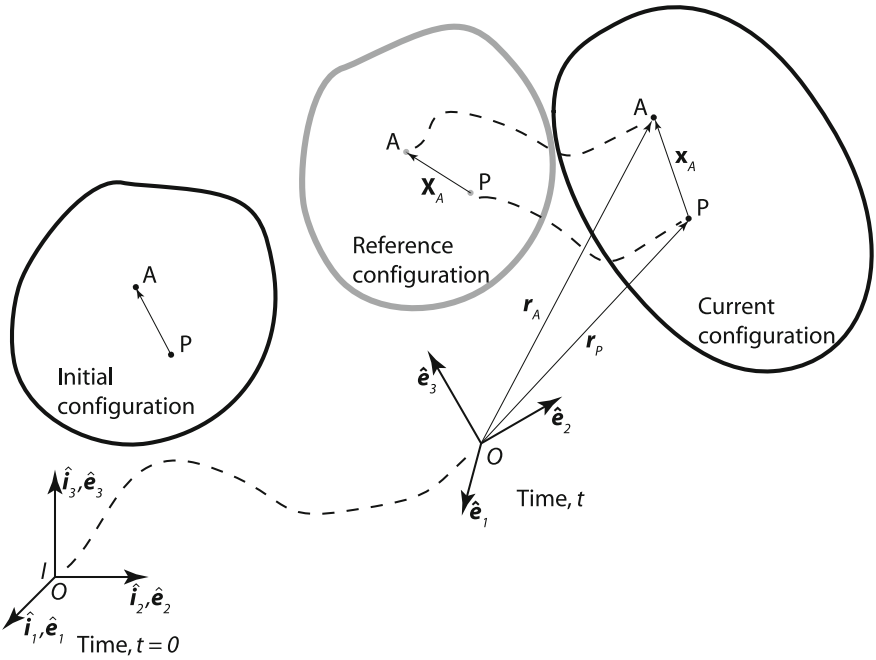

Fig. 2.1 The motion of deformable body as described in a fixed frame $\mathscr{I}$, and a translating and rotating frame $\mathscr{O}$. The motion begins at time $t = 0$ when both $\mathscr{I}$ and $\mathscr{O}$ are aligned. The reference configuration in $\mathscr{O}$ is shown as a thick *gray curve*. This is obtained as an image of the body's initial configuration that moves along with $\mathscr{O}$. *Dashed lines* trace the paths of various points. While O's path is observed in $\mathscr{I}$, the paths of A and P are followed in $\mathscr{O}$

$\mathscr{O}$. The reference point is introduced with an eye to future applications, wherein we will often seek to separate a body's motion into that of its center of mass, and motion relative to the mass center. Though $\mathbf{X}_A$ and $\mathbf{x}_A(t)$ are relative position vectors, for brevity we will address them as the reference and current locations of a point A. At any time, A's location with respect to O is

$$\mathbf{r}_A(t) = \mathbf{r}_P(t) + \mathbf{x}_A(t). \tag{2.9}$$

Even though in a fixed frame $\mathbf{X}_A$ is rotating along with $\mathscr{O}$, it appears fixed in $\mathscr{O}$, so that we suppress its time dependance.

The current location $\mathbf{x}_A(t)$ of a material point will in general evolve as some function that depends on both time t, and its reference position $\mathbf{X}_A$, i.e.,

$$\mathbf{x}_A(t) = \mathbf{f}\left(\mathbf{X}_A, t\right), \tag{2.10}$$

where $\mathbf{f}$ is an invertible, sufficiently smooth, vector valued function of space and time.[1] Thus,

$$\mathbf{r}_A(t) = \mathbf{r}_P(t) + \mathbf{f}(\mathbf{X}_A, t). \tag{2.11}$$

Differentiating (2.9) repeatedly with respect to time in $\mathscr{O}$ we may compute the material point A's velocity $\mathbf{v}_A$ and acceleration $\mathbf{a}_A$ relative to $\mathscr{O}$.

2.4 Simple Motions

We now describe some motions that will be employed extensively in later chapters. These are obtained by specializing $\mathbf{f}$ to be particularly simple functions of $\mathbf{X}_A$.

2.4.1 Example 1: Pure Rotation

Consider a body that moves in a manner such that there is a reference point P on the body that always lies at the origin of $\mathscr{O}$. Then, $\mathbf{r}_P(t) = \mathbf{0}$. Furthermore, let the mapping

$$\mathbf{f}(\mathbf{X}_A, t) \equiv \mathsf{R}(t) \cdot \mathbf{X}_A, \tag{2.12}$$

where R is a rotation tensor. Then, from (2.10) and (2.11), the location at time t of any point A in the body is

$$\mathbf{r}_A(t) = \mathbf{x}_A(t) = \mathsf{R}(t) \cdot \mathbf{X}_A. \tag{2.13}$$

This motion represents rotation of the body as a *rigid* entity about O. Indeed, the distance between any two points A and B remains the same:

$$|\mathbf{r}_A - \mathbf{r}_B| = |\mathsf{R} \cdot (\mathbf{X}_A - \mathbf{X}_B)| = |\mathsf{R}|\,|\mathbf{X}_A - \mathbf{X}_B| = |\mathbf{X}_A - \mathbf{X}_B|.$$

It is now possible to introduce a coordinate system $\left\{\mathscr{P}, \hat{\mathbf{e}}'_i\right\}$ whose origin coincides with O and which rotates so that $\hat{\mathbf{e}}'_i = \mathsf{R} \cdot \hat{\mathbf{e}}_i$. Then in $\mathscr{P}$ the body will appear fixed. Further kinematics may now be developed as in Sects. 2.2.1 and 2.2.2.

We begin by introducing the angular velocity tensor

$$\Omega_P(t) = \dot{\mathsf{R}}(t) \cdot \mathsf{R}^T(t), \tag{2.14}$$

whose axial vector $\boldsymbol{\omega}_P(t)$ now represents the angular velocity of the frame $\mathscr{P}$, and, hence, also that of the body, in frame $\mathscr{O}$. Differentiating (2.13) with respect to time

[1] For more information about conditions that $\mathbf{f}$ is subjected to we refer the interested reader to Gurtin (1981, Chap. III).

(in $\mathscr{O}$) , and proceeding as in (2.3), we find A's velocity in $\mathscr{O}$ to be

$$\mathbf{v}_A = \Omega_P \cdot \mathbf{x}_A(t) = \boldsymbol{\omega}_P \times \mathbf{x}_A(t). \tag{2.15}$$

For A's acceleration, we differentiate (2.15), to obtain

$$\mathbf{a}_A(t) = \dot{\Omega}_P \cdot \mathbf{x}_A + \Omega_P \cdot \mathbf{v}_A = (\dot{\Omega}_P + \Omega_P^2) \cdot \mathbf{x}_A = \dot{\boldsymbol{\omega}}_P \times \mathbf{x}_A + \boldsymbol{\omega}_P \times \{\boldsymbol{\omega}_P \times \mathbf{x}_A\}, \tag{2.16}$$

where in the last step (1.18) has been utilized. The first term on the right is the *angular acceleration*, while the second is the *centripetal acceleration*. Once the velocity and acceleration of point A are known in $\mathscr{O}$, we may utilize (2.8) to find their inertial values.

2.4.2 Example 2: General Rigid Body Motion

A rigid body cannot deform. However, it can translate and rotate. By Chasles' theorem, the general motion of a rigid body is a combination of a pure rotation about a point of the body, and the translational motion of that point; see Greenwood (1988, p. 341). This latter point may be arbitrary, but is usually taken to be the center of mass of the body, say, P. Combining Chasles' theorem with the previous example, we find the motion of point A as

$$\mathbf{r}_A(t) = \mathbf{r}_P(t) + \mathsf{R}(t) \cdot \mathbf{X}_A, \tag{2.17}$$

where R is some rotation tensor. The above is another instance of (2.10) with the same mapping $\mathbf{f}$ as in (2.12). The two terms on the right hand side represent pure rotation about the center of mass (see the previous example), and the mass center's motion, respectively. At any time t, the above motion is an example of an *affine transformation*.

The velocities and accelerations relative to the rotating frame $\mathscr{O}$ are obtained by simply adding the motion of P to the formulae obtained in the previous example, viz.,

$$\mathbf{v}_A = \mathbf{v}_P + \Omega_P \cdot \mathbf{x}_A = \mathbf{v}_P + \boldsymbol{\omega}_P \times \mathbf{x}_A \tag{2.18a}$$

and

$$\begin{aligned} \mathbf{a}_A &= \mathbf{a}_P + (\dot{\Omega}_P + \Omega_P^2) \cdot \mathbf{x}_A \\ &= \mathbf{a}_P + \dot{\boldsymbol{\omega}}_P \times \mathbf{x}_A + \boldsymbol{\omega}_P \times \{\boldsymbol{\omega}_P \times \mathbf{x}_A\}, \end{aligned} \tag{2.18b}$$

where $\mathbf{v}_P = \dot{\mathbf{r}}_P$ and $\mathbf{a}_P = \ddot{\mathbf{r}}_P$ are the velocity and acceleration of P, respectively, and Ω is the angular velocity tensor of the body given by (2.14). The second term in the expression of $\mathbf{v}_A$ and the last two terms of $\mathbf{a}_A$ capture, respectively, A's velocity and acceleration relative to an observer at P who rotates with frame $\mathscr{O}$. The formulae above are familiar to us from rigid body mechanics.

2.4.3 Example 3: Homogeneous Motion

Consider again the body of Example 1 that is pinned at P. We generalize the pure rotational motion prescribed in that example by replacing the rotational tensor $\mathsf{R}(t)$ in (2.13) by a tensor $\mathsf{H}(t)$. The motion relative to frame $\mathscr{O}$ of the material point A is then

$$\mathbf{r}_A(t) = \mathbf{x}_A(t) = \mathsf{H}(t) \cdot \mathbf{X}_A =: \mathbf{f}(\mathbf{X}_A, t). \tag{2.19}$$

The above defines *homogeneous motion*. The tensor H, while invertible and having $\det \mathsf{H} > 0$ for all time, does not have any other specific properties like symmetry, orthogonality, etc. The above is a time-dependent *linear* mapping of $\mathbf{X}_A$ to $\mathbf{x}_A$, and is the simplest three-dimensional generalization of rigid-body-like rotational motion to include material deformation. It has been previously studied by Slawianowski (1974, 1975) and Cohen (1981), and, from the viewpoint of rational mechanics, by Cohen and Muncaster (1988).

Proceeding in a manner analogous to the previous two examples, a material point A's velocity and acceleration as observed in $\mathscr{O}$ are, respectively,

$$\mathbf{v}_A(t) = \dot{\mathsf{H}} \cdot \mathbf{X}_A \quad \text{and} \quad \mathbf{a}_A(t) = \ddot{\mathsf{H}} \cdot \mathbf{X}_A. \tag{2.20}$$

We will develop further insight into this motion in Sect. 2.6.1.

2.4.4 Example 4: Affine Motion

Finally, consider a motion in which the center of mass P of the body translates with respect to frame $\mathscr{O}$, while the body itself deforms in a homogeneous manner about P, i.e.,

$$\mathbf{r}_A(t) = \mathsf{H}(t) \cdot \mathbf{X}_A + \mathbf{r}_P(t), \tag{2.21}$$

where $\mathbf{r}_P(t)$ locates P. The above defines a general *affine motion*. The velocity and acceleration of some point A are obtained by simply augmenting the corresponding expressions for homogeneous deformation with P's velocity $\mathbf{v}_P(t)$ and acceleration $\mathbf{a}_P(t)$ in $\mathscr{O}$, respectively, viz.,

$$\mathbf{v}_A(t) = \dot{\mathsf{H}}(t) \cdot \mathbf{X}_A + \mathbf{v}_P(t) \quad \text{and} \quad \mathbf{a}_A(t) = \ddot{\mathsf{H}} \cdot \mathbf{X}_A + \mathbf{a}_P(t). \tag{2.22}$$

We will return to this motion in greater detail in Sect. 2.6.2.

Internal force distribution in most materials depends on the nature of the deformation and/or its rate in the neighborhood of a material point, say A. This we analyze next.

2.5 Local Motion

The change in the length and orientation of an infinitesimal material fiber $\delta\mathbf{X}_A$ at point A may be approximated by the first term in a Taylor series expansion of (2.10):

$$\delta\mathbf{x}_A \approx \mathsf{F}(\mathbf{X}_A, t) \cdot \delta\mathbf{X}_A, \tag{2.23}$$

where the *deformation gradient tensor*

$$\mathsf{F}(\mathbf{X}, t) = \frac{\partial \mathbf{x}}{\partial \mathbf{X}} = \frac{\partial \mathbf{f}}{\partial \mathbf{X}}. \tag{2.24}$$

It is clear that in this the motion of the reference point P will not play a role. The deformation gradient F is a *homogeneous* mapping of the infinitesimal material line element $\delta\mathbf{X}_A$ in the reference configuration to the stretched and/or rotated $\delta\mathbf{x}_A$; cf. Fig. 2.1. The tensor F is identity if the infinitesimal material line element $\delta\mathbf{X}_A$ translates without rotating or stretching and, so, quantifies relative motion in the neighborhood of A. Ignoring crack/void openings and/or material interpenetration allows us to assume that F is invertible, so that

$$\mathsf{F}^{-1}(\mathbf{x}, t) = \frac{\partial \mathbf{X}}{\partial \mathbf{x}}. \tag{2.25}$$

In fact, $\det \mathsf{F} > 0$ as we will see in Sect. 2.5.1.

Applying the polar decomposition theorem (1.27) to F, we find that

$$\mathsf{F} = \mathsf{R}_F \cdot \mathsf{U} = \mathsf{V} \cdot \mathsf{R}_F, \tag{2.26}$$

with R_F being a rotation tensor,[2] and U and V are symmetric, positive-definite tensors called the *right-* and *left- stretch tensors*, respectively. Employing this decomposition in (2.23) suggests that the local motion of a material element may be viewed as *local deformation* given by U followed by *local rotation* due to R_F, or, equivalently, as *local rotation* due to R_F followed by *local deformation* given by V.

The tensors U and V, being symmetric, may be described completely by their three eigenvectors and the related three eigenvalues. From the previous two equations, it is easy to see that an infinitesimal fiber that lies along any principal axis of U, or V, is not rotated by these tensors; it extends or shortens by an amount given by the corresponding eigenvalue. Any rotation that this fiber experiences is due to R_F. Two infinitesimal fibers emanating from the same point will be rotated by U or V by different amounts, unless they lie along these tensors' principal axes. This difference in rotation changes the initial angle between these two fibers, thereby constituting a *shear*. Again, R_F rotates both these fibers by the same amount without any shearing.

[2] The subscript 'F' is included to distinguish this rotation tensor from R defined by (2.1) that relates frames $\mathscr{O}$ and $\mathscr{I}$.

Clearly, any symmetric tensor will have the same effect on material fibers as U and V. For this reason, motion due to symmetric tensors, like U and V above, constitutes a *pure deformation*.

Finally, it is clear that when observed in a fixed frame, say $\mathscr{I}$, a rigid-body motion corresponding to the motion of the frame $\mathscr{O}$ will precede the local deformation. Thus, the deformation gradient F^I, relating the initial and current configurations in Fig. 2.1, will be related to F by

$$\mathsf{F}^I = \mathsf{F} \cdot \mathsf{R}, \tag{2.27}$$

where R defined by (2.1) relates $\mathscr{O}$ and $\mathscr{I}$.

2.5.1 Strain. Surface Change. Volume Change

We saw above that the deformation gradient F provides information of the local motion. However, it is *not* a suitable measure for the local deformation, or *strain*. Because no deformation takes place when only rotation is present, any strain measure should have the attribute that it remains unaffected by rigid body rotation, and, as we see from (2.26), F does not share this property. Tensors may be constructed that do, however, remain unaffected by local rigid-body rotation. Two important examples are the *right-* and *left- Cauchy–Green tensors*, respectively,

$$\mathsf{C} = \mathsf{F}^T \cdot \mathsf{F} = \mathsf{U}^2 \quad \text{and} \quad \mathsf{B} = \mathsf{F} \cdot \mathsf{F}^T = \mathsf{V}^2.$$

From these appropriate strain measures may be constructed and we refer the interested reader to Spencer (1980, Sect. 6.4). We will not have reason here to utilize these strain measures here. To us more important will be the rate at which straining occurs, and this is explored in the next section.

We will, however, require changes in surface and volume material elements. Consider an infinitesimal patch of area $\mathrm{d}S_0$ oriented by the unit vector $\hat{\mathbf{N}}$ that under some motion $\mathbf{f}(\mathbf{X}, t)$ deforms into another area element $\mathrm{d}S$ with normal $\hat{\mathbf{n}}$. To relate stresses and tractions[3] known in the current configuration in terms of the reference coordinates, and vice versa, we will require to know how $\mathrm{d}S_0$ and $\hat{\mathbf{N}}$ relate to $\mathrm{d}S$ and $\hat{\mathbf{n}}$, respectively. It may be shown (Spencer 1980, pp. 123–125) that

$$\frac{\mathrm{d}S}{\mathrm{d}S_0} = \frac{\det \mathsf{F}}{\left(\hat{\mathbf{n}} \cdot \mathsf{B} \cdot \hat{\mathbf{n}}\right)^{1/2}} = \det \mathsf{F} \left(\hat{\mathbf{N}} \cdot \mathsf{C}^{-1} \cdot \hat{\mathbf{N}}\right)^{1/2}, \tag{2.28a}$$

$$\hat{\mathbf{N}} = \frac{\hat{\mathbf{n}} \cdot \mathsf{F}}{\det \mathsf{F}} \left(\frac{\mathrm{d}S}{\mathrm{d}S_0}\right)^{-1} \quad \text{and} \quad \hat{\mathbf{n}} = \frac{\mathsf{F}^{-T} \cdot \hat{\mathbf{N}}}{(\det \mathsf{F})^{-1}} \left(\frac{\mathrm{d}S}{\mathrm{d}S_0}\right)^{-1}. \tag{2.28b}$$

[3] Cf. (2.54).

The above allows us to relate surface integrals over a body's current surface S into integrals in reference coordinates, e.g.,

$$\int_S \Phi(\mathbf{x}(t), t) \cdot \hat{\mathbf{n}} \, \mathrm{d}S = \int_{S_0} \Phi_0(\mathbf{X}, t) \cdot \mathsf{F}^{-T} \cdot \hat{\mathbf{N}} \, (\det \mathsf{F}) \, \mathrm{d}S_0, \tag{2.29}$$

where Φ is an nth-order tensor field, $\Phi_0(\mathbf{X}, t) = \Phi_0\left(\mathbf{f}^{-1}(\mathbf{x}, t), t\right) = \Phi(\mathbf{x}, t)$, and S_0 is the surface of the reference configuration.

In a similar spirit, consider relating an initial infinitesimal volume $\mathrm{d}V_0$ with its final image $\mathrm{d}V$ at time t during a motion $\mathbf{f}(\mathbf{X}, t)$. Spencer (1980, p. 91–93) proves that

$$\Delta := \frac{\mathrm{d}V}{\mathrm{d}V_0} = \det \mathsf{F}; \tag{2.30}$$

Δ is also called the *dilatation*. Readers familiar with transformation of three-dimensional integrals will immediately identify $\det \mathsf{F}$ with the *Jacobian* of the mapping $\mathbf{f}$. Because mass of the infinitesimal element is conserved, if ρ_0 and ρ are the initial and final densities, we must have $\rho_0 \mathrm{d}V_0 = \rho \mathrm{d}V$. Employing (2.30), we obtain the relation

$$\rho_0 = \rho \frac{\mathrm{d}V}{\mathrm{d}V_0} = \rho \det \mathsf{F}. \tag{2.31}$$

From the above formulae, because density and volume changes cannot be negative, we must have that $\det \mathsf{F} > 0$.

As for surface integrals earlier, the above relation allows us to transform the volume integral of the tensor field $\Phi_0(\mathbf{x}, t)$ from current to reference coordinates:

$$\int_V \Phi(\mathbf{x}(t), t) \mathrm{d}V = \int_{V_0} \Phi_0(\mathbf{X}, t) \det \mathsf{F} \, \mathrm{d}V_0, \tag{2.32}$$

where the current V and reference V_0 are related by $\mathbf{f}$. An important particular instance is when Φ is weighted by the density ρ, i.e., $\Phi(\mathbf{x}, t) = \Psi(\mathbf{x}, t)\rho(\mathbf{x}, t)$. In this case, (2.31) simplifies the volume integral transformation to

$$\int_V \Psi(\mathbf{x}, t)\rho(\mathbf{x}(t), t) \mathrm{d}V = \int_{V_0} \Psi_0(\mathbf{X}, t)\rho_0(\mathbf{X}), \mathrm{d}V_0, \tag{2.33}$$

where $\Psi_0(\mathbf{X}, t) = \Psi_0\left(\mathbf{f}^{-1}(\mathbf{x}, t), t\right) = \Psi(\mathbf{x}, t)$.

2.5.2 *Rate of Local Motion*

In a dynamic situation, the rate at which material deforms, i.e., the *strain rate*, is important. The stress response of many materials, like fluids and flowing granular

materials, depends on the rate of local deformation, and not on how much the material has deformed from an initial unstressed state. We now develop measures of local strain rate.

Differentiating (2.23) in $\mathscr{C}$, the rate of local deformation at a material point A is

$$\frac{\mathrm{d}(\delta \mathbf{x}_A)}{\mathrm{d}t} = \dot{\mathsf{F}} \cdot \delta \mathbf{X}_A = \dot{\mathsf{F}} \cdot \mathsf{F}^{-1} \cdot \delta \mathbf{x}_A = \mathsf{L} \cdot \delta \mathbf{x}_A,$$

where the quantity

$$\mathsf{L} = \dot{\mathsf{F}} \cdot \mathsf{F}^{-1} \tag{2.34}$$

is the *velocity gradient tensor* that relates the local deformation rate to the current configuration. This is clear, when we note that

$$\dot{\mathsf{F}} = \frac{\mathrm{d}}{\mathrm{d}t}\left(\frac{\partial \mathbf{x}}{\partial \mathbf{X}}\right) = \frac{\partial \mathbf{v}}{\partial \mathbf{X}} \quad \text{and} \quad \mathsf{F}^{-1} = \frac{\partial \mathbf{X}}{\partial \mathbf{x}},$$

with $\mathbf{v}(\mathbf{x}, t) = \mathrm{d}\mathbf{x}(t)/\mathrm{d}t$. Thus, the previous equation yields

$$\mathsf{L} = \frac{\partial \mathbf{v}}{\partial \mathbf{X}} \cdot \frac{\partial \mathbf{X}}{\partial \mathbf{x}} = \frac{\partial \mathbf{v}}{\partial \mathbf{x}} = \nabla_{\mathbf{x}} \mathbf{v}, \tag{2.35}$$

where the subscript on ∇ indicates the differentiation variable.

The deformation gradient F included contributions from both local rotation and local deformation; cf. (2.26). Similarly, the velocity gradient L is comprised of a local spin and a local stretch rate. This is easily seen by following (1.17) and writing

$$\mathsf{L} = \mathsf{D} + \mathsf{W}, \tag{2.36}$$

in terms of the symmetric *strain rate tensor*

$$\mathsf{D} = \frac{1}{2}\left(\mathsf{L} + \mathsf{L}^T\right) = \operatorname{sym} \mathsf{L}, \tag{2.37}$$

and the anti-symmetric *spin tensor*

$$\mathsf{W} = \frac{1}{2}\left(\mathsf{L} - \mathsf{L}^T\right) = \operatorname{asym} \mathsf{L}. \tag{2.38}$$

Again, infinitesimal material elements along any principal axis of D do not rotate; their strain rate is governed by D's eigenvalues. The *spin* vector $\mathbf{w}$ associated with W gives the local material angular velocity, so that, given any fiber $\delta \mathbf{x}_A$,

$$\mathsf{W}(\mathbf{x}_A, t) \cdot \delta \mathbf{x}_A = \mathbf{w}(\mathbf{x}_A, t) \times \delta \mathbf{x}_A.$$

The rate of change of F was measured in the rotating frame $\mathscr{O}$. As laws of motion are in terms of time derivatives taken in the inertial frame $\mathscr{I}$, let us compute the rate of change in $\mathscr{I}$ of the deformation gradient observed in $\mathscr{I}$, i.e., $\mathring{\mathsf{F}}^I$. Differentiating formula (2.27), and employing (2.2), (2.6) and (2.34) we find that

$$\mathring{\mathsf{F}}^I = \mathring{\mathsf{F}} \cdot \mathsf{R} + \mathsf{F} \cdot \mathring{\mathsf{R}} = \left(\dot{\mathsf{F}} + \Omega \cdot \mathsf{F} - \mathsf{F} \cdot \Omega\right) \cdot \mathsf{R} + \mathsf{F} \cdot \Omega \cdot \mathsf{R} = (\mathsf{L} + \Omega) \cdot \mathsf{F} \cdot \mathsf{R},$$

so that the velocity gradient observed in $\mathscr{I}$ is

$$\tilde{\mathsf{L}} := \mathring{\mathsf{F}}^I \cdot \left(\mathsf{F}^I\right)^{-1} = \mathsf{L} + \Omega. \tag{2.39}$$

Thus, the velocity gradient in $\mathscr{O}$ differs from that in $\mathscr{I}$ only by the rotation rate of $\mathscr{O}$. The above formula may be obtained far more directly by first recognizing that $\tilde{\mathsf{L}} = \nabla_{\mathbf{x}} \mathbf{v}^I$ and then replacing for $\mathbf{v}^I$ from (2.8).

Employing formula (1.45c), and definitions (2.30) and (2.34), we find that

$$\dot{\Delta} = \Delta \operatorname{tr} \mathsf{L} = \Delta \operatorname{tr} \mathsf{D} = \Delta \operatorname{tr} \nabla_{\mathbf{x}} \mathbf{v}(\mathbf{x}, t) = \Delta \, \nabla_{\mathbf{x}} \cdot \mathbf{v}(\mathbf{x}, t), \tag{2.40}$$

where we note that $\operatorname{tr} \mathsf{L} = \operatorname{tr} \mathsf{D}$, because $\operatorname{tr} \mathsf{W} = 0$. Similarly, differentiating (2.31) gives

$$\dot{\rho} = -\rho \operatorname{tr} \mathsf{D}. \tag{2.41}$$

Note that as Δ and ρ are scalars, their rates of change in $\mathscr{I}$ are the same as above.

2.5.3 *Transport Theorem. Mass Balance*

Frequently, we will require to evaluate the quantity

$$\frac{\mathrm{d}}{\mathrm{d}t} \int_V \Phi(\mathbf{x}(t), t) \, \mathrm{d}V,$$

where Φ may be a scalar, a vector, a second-order tensor or some other higher-order tensorial field, and the integral is over a current volume V within the body moving/deforming according to the motion $\mathbf{f}(\mathbf{X}, t)$. Employing (2.32), we compute

$$\begin{aligned} \frac{\mathrm{d}}{\mathrm{d}t} \int_V \Phi(\mathbf{x}(t), t) \, \mathrm{d}V &= \frac{\mathrm{d}}{\mathrm{d}t} \int_{V_0} \Phi_0(\mathbf{X}, t) \det \mathsf{F} \, \mathrm{d}V_0 = \int_{V_0} \frac{\mathrm{d}}{\mathrm{d}t} \{\Phi_0(\mathbf{X}, t) \det \mathsf{F}\} \, \mathrm{d}V_0 \\ &= \int_V \frac{\mathrm{d}}{\mathrm{d}t} \{\Phi(\mathbf{x}(t), t) \det \mathsf{F}\} \, (\det \mathsf{F})^{-1} \, \mathrm{d}V, \end{aligned}$$

where Φ_0 is defined as in the previous section, and we brought the differentiation within the integral as V_0 is fixed in $\mathscr{O}$. The differentiation may be carried out via the

chain rule and formulae (1.45c), (1.47) and (2.34) to yield

$$\frac{\mathrm{d}}{\mathrm{d}t}\{\Phi \det \mathsf{F}\} = \left[\dot{\Phi} + \Phi \operatorname{tr}\left(\dot{\mathsf{F}} \cdot \mathsf{F}^{-1}\right)\right] \det \mathsf{F} = \left[\frac{\partial \Phi}{\partial t} + \nabla_{\mathbf{x}}\Phi \cdot \mathbf{v} + \Phi(\operatorname{tr} \mathsf{L})\right] \det \mathsf{F},$$

so that, recalling from (2.34) that $\operatorname{tr} \mathsf{L} = \nabla_{\mathbf{x}} \cdot \mathbf{v}$, we finally obtain

$$\frac{\mathrm{d}}{\mathrm{d}t}\int_V \Phi(\mathbf{x}(t), t)\,\mathrm{d}V = \int_V \left[\frac{\partial \Phi}{\partial t} + \nabla_{\mathbf{x}}\Phi \cdot \mathbf{v} + \Phi \nabla_{\mathbf{x}} \cdot \mathbf{v}\right] \mathrm{d}V. \tag{2.42}$$

The above is the *transport theorem* for volume integrals of any tensorial field $\Phi(\mathbf{x}, t)$. Similar versions for line and surface integrals may be derived; see, e.g., Asaro and Lubarda (2006, p. 83).

We illustrate the transport theorem by deriving the condition that assures that mass be conserved. To this end, we consider an initial region of volume V_0 within a body of density $\rho_0(\mathbf{X})$ that at some time t is mapped to another region with volume V and density $\rho(\mathbf{x}, t)$ by the motion $\mathbf{f}(\mathbf{X}, t)$. Because the mass of the region remains unchanged, we must have

$$\frac{\mathrm{d}}{\mathrm{d}t}\int_V \rho(\mathbf{x}(t), t)\,\mathrm{d}V = 0.$$

Employing (2.42) with $\Phi = \rho$, the above yields

$$\int_V \left[\frac{\partial \rho}{\partial t} + \nabla_{\mathbf{x}}\rho \cdot \mathbf{v} + \rho \nabla_{\mathbf{x}} \cdot \mathbf{v}\right] \mathrm{d}V = 0,$$

which, because the choice of the original region V was arbitrary, is equivalent to

$$\frac{\partial \rho}{\partial t} + \nabla_{\mathbf{x}}\rho \cdot \mathbf{v} + \rho \nabla_{\mathbf{x}} \cdot \mathbf{v} = \frac{\partial \rho}{\partial t} + \nabla_{\mathbf{x}} \cdot (\rho \mathbf{v}) = 0. \tag{2.43}$$

The above is the *continuity equation* that enforces mass conservation. In case of an *incompressible* body, a material element's density remains constant, so that $\dot{\rho}(\mathbf{x}, t) = \partial\rho/\partial t + \nabla_{\mathbf{x}}\rho \cdot \mathbf{v} = 0$, and the continuity equation simplifies to

$$\nabla_{\mathbf{x}} \cdot \mathbf{v} = \operatorname{tr} \mathsf{L} = \operatorname{tr} \mathsf{D} = 0. \tag{2.44}$$

A special, but important class of integrals involve a field Φ weighted by the body's density, i.e., $\Phi = \Psi\rho$; cf. (2.33). In this case, employing (2.33) twice, we have

$$\begin{aligned}\frac{\mathrm{d}}{\mathrm{d}t}\int_V \Psi(\mathbf{x}(t), t)\rho(\mathbf{x}, t)\,\mathrm{d}V &= \frac{\mathrm{d}}{\mathrm{d}t}\int_{V_0} \Psi_0(\mathbf{X}, t)\rho_0(\mathbf{X})\,\mathrm{d}V_0 = \int_{V_0} \dot{\Psi}_0(\mathbf{X}, t)\rho_0(\mathbf{X})\,\mathrm{d}V_0 \\ &= \int_V \dot{\Psi}(\mathbf{x}(t), t)\rho(\mathbf{x}, t)\,\mathrm{d}V,\end{aligned} \tag{2.45}$$

where Ψ_0 has the same meaning as in the previous section, and the overdot denotes $\mathrm{d}/\mathrm{d}t$, the total, and *not* the partial derivative with respect to time in $\mathscr{O}$. Thus, the differential operator moves inside the integral in spite of a time-varying V.

2.6 Further Analysis of Simple Motions

We return to the simple motions considered earlier in Sect. 2.4. We further investigate homogeneous and affine motions employing deformation and deformation rate measures introduced above. As always, we follow motion in the rotating frame $\mathscr{O}$.

2.6.1 Example 3: Homogeneous Motion

We develop further insight into this motion by evaluating the deformation gradient via (2.24) and (2.19), to obtain

$$\mathsf{F}(t) = \mathsf{H}(t). \tag{2.46}$$

Thus $\det \mathsf{H}$, which, recall from (2.30), equals the change in volume, cannot vanish or be negative. The deformation gradient at a point depends only on time, and not on that point's location – it is *homogeneous* in space. This explains why the motion (2.19) is called *homogenous deformation*. The behavior local to a material point at the origin – which may be the center of mass – is replicated on a global scale, and we do not have to resort to infinitesimal line elements to investigate this deformation.

From (2.34), we obtain the velocity gradient in $\mathscr{O}$ as

$$\mathsf{L} = \dot{\mathsf{H}} \cdot \mathsf{H}^{-1}. \tag{2.47}$$

The strain rate and spin tensors, $\mathsf{D} = \operatorname{sym}(\dot{\mathsf{H}} \cdot \mathsf{H}^{-1})$ and $\mathsf{W} = \operatorname{asym}(\dot{\mathsf{H}} \cdot \mathsf{H}^{-1})$, are obtained from (2.37) and (2.38), respectively. All these tensors, like the deformation gradient, do not depend at any fixed time on a material point's location; they too are homogeneous. The velocity and acceleration of a material point A in $\mathscr{O}$ were computed in Sect. 2.4. Employing (2.47), these may now be rewritten as

$$\mathbf{v}_A = \mathsf{L} \cdot \mathbf{x}_A \tag{2.48a}$$

and

$$\mathbf{a}_A = \dot{\mathsf{L}} \cdot \mathbf{x}_A + \mathsf{L} \cdot \mathbf{v}_A = (\dot{\mathsf{L}} + \mathsf{L}^2) \cdot \mathbf{x}_A, \tag{2.48b}$$

Because $\mathsf{L} = \mathsf{D} + \mathsf{W}$, the above formulae may be expanded as

$$\mathbf{v}_A = (\mathsf{D} + \mathsf{W}) \cdot \mathbf{x}_A \tag{2.49a}$$

and

$$\mathbf{a}_A = (\dot{\mathsf{D}} + \mathsf{D}^2) \cdot \mathbf{x}_A + (\mathsf{D} \cdot \mathsf{W} + \mathsf{W} \cdot \mathsf{D}) \cdot \mathbf{x}_A + (\dot{\mathsf{W}} + \mathsf{W}^2) \cdot \mathbf{x}_A. \tag{2.49b}$$

We may identify $\mathbf{w}(t)$ as W's axial vector, and $\mathbf{w}(t)$ then is the *angular velocity* of any material line of the body. Because $\mathbf{w}(t)$ is homogeneous, every material line rotates at the same rate. However, neighboring line elements may shear with respect to each other due to possibly different strain rates.

A homogeneous deformation has the important property that it deforms ellipsoids into ellipsoids, i.e., given an initially ellipsoidal body, its shape at any time as it evolves according to (2.19) will be an ellipsoid, albeit a rotated, stretched and sheared version of the original ellipsoid. This may be proved as follows. An ellipsoid's surface is given by the equation

$$\mathbf{X} \cdot \mathsf{E} \cdot \mathbf{X} = 1,$$

where E is a constant symmetric positive-definite tensor.[4] At any time t the material point located by $\mathbf{X}$ gets mapped to $\mathbf{x}(t) = \mathsf{H}(t) \cdot \mathbf{X}$, so that $\mathbf{X} = \mathsf{H}^{-1}(t) \cdot \mathbf{x}(t)$. Substituting this in the above equation, we obtain

$$(\mathsf{H}^{-1} \cdot \mathbf{x}) \cdot \mathsf{E} \cdot (\mathsf{H}^{-1} \cdot \mathbf{x}) = 1.$$

Manipulating the above by an application of (1.11) finally yields

$$\mathbf{x}(t) \cdot \mathsf{e}(t) \cdot \mathbf{x}(t) = 1$$

as the shape of the deformed surface, where

$$\mathsf{e}(t) = \mathsf{H}^{-T}(t) \cdot \mathsf{E} \cdot \mathsf{H}^{-1}(t). \tag{2.50}$$

Recognizing that $\mathsf{e}(t)$ is for all times a positive-definite symmetric tensor,[5] we see that the deformed surface is also an ellipsoid.

In future applications, we will exclusively consider ellipsoidal bodies. It is helpful therefore to also derive the rate of change of this latter ellipsoid. This is accomplished by differentiating $\mathsf{E} = \mathsf{H}^T \cdot \mathsf{e} \cdot \mathsf{H}$ obtained by inverting (2.50), employing $\mathsf{L} = \dot{\mathsf{H}} \cdot \mathsf{H}^{-1}$, and solving for $\dot{\mathsf{e}}(t)$. We find,

$$\dot{\mathsf{e}} = -\left(\mathsf{e} \cdot \mathsf{L} + \mathsf{L}^T \cdot \mathsf{e}\right) = -2\,\mathrm{sym}\,(\mathsf{e} \cdot \mathsf{L}) = -2\,\mathrm{sym}\,(\mathsf{e} \cdot \mathsf{D}) - 2\,\mathrm{sym}\,(\mathsf{e} \cdot \mathsf{W}).$$

The mapping (2.50) is *not* in general an orthogonal transformation, i.e., the eigenvalues for $\mathsf{e}(t)$ and E are often different, and the principal axes of E are *not* always mapped to the principal axes of $\mathsf{e}(t)$. In addition to being rotated, the initial ellipsoid is *stretched* and *sheared* by the transformation $\mathsf{H}(t)$. The principal axes coordinate

[4] Indeed, such an E is expressible as $\mathsf{E} = \sum_{i=1}^{3} \lambda_i^2 \hat{\mathbf{E}}_i \otimes \hat{\mathbf{E}}_i$, where λ_i^2 are the eigenvalues and $\hat{\mathbf{E}}_i$ are the corresponding eigenvectors. Then $1 = \mathbf{X} \cdot \mathsf{E} \cdot \mathbf{X} = \lambda_i^2 X_i^2$ represents an ellipsoid with semi-axes of length λ_i^{-1} lying along $\hat{\mathbf{E}}_i$.

[5] While symmetry is obvious, the following computation shows that e is positive definite. For arbitrary $\mathbf{u}$, we have $\mathbf{u} \cdot \mathsf{e} \cdot \mathbf{u} = \mathbf{u} \cdot \mathsf{H}^{-T} \cdot \mathsf{E} \cdot \mathsf{H}^{-1} \cdot \mathbf{u} = \left(\mathsf{H}^{-1} \cdot \mathbf{u}\right) \cdot \mathsf{E} \cdot \left(\mathsf{H}^{-1} \cdot \mathbf{u}\right) = \mathbf{y} \cdot \mathsf{E} \cdot \mathbf{y} > 0$, as E is positive definite and H is invertible.

system of the current and original ellipsoids, being orthogonal, instead relate through a time-varying rotation tensor, say $\mathsf{R}_e(t)$. This defines an associated *angular velocity tensor* $\Omega_e(t) = \dot{\mathsf{R}}_e(t) \cdot \mathsf{R}_e^T(t)$. The angular velocity of the evolving ellipsoid's principal axes coordinate system is, thus, given by the axial vector $\boldsymbol{\omega}_e$ of Ω_e. The crucial detail to note is that $\boldsymbol{\omega}_e$ does *not* necessarily equal $\mathbf{w}$ defined via (2.38) – the principal axes of the ellipsoid may rotate at a rate different from that of a material line. In other words, the semi-major axes of a homogeneously deforming ellipsoid are *not* usually material lines. This is because, in such an ellipsoid, material lines extend/shorten as they rotate. The amount of strain experienced depends on the orientation of the material line with respect to the eigenvectors of the strain rate tensor D. If, at any instant, D's eigenvectors do not align with those of e, i.e., the principal axes of the current ellipsoid, shearing in the neighborhood of a semi-major axis will cause an adjacent material line to become longer than the one lying along the present semi-major axis. Recall that if two line elements are not collinear with the eigenvectors of D, they get sheared.

2.6.2 Example 4: Affine Motion

Recall from Sect. 2.6.2 that an affine motion consists of homogeneous deformation about a reference point that may itself move. An initial ellipsoid deforms into another, possibly rotated, stretched and sheared ellipsoid, while the reference point – possibly the center of mass – follows some general path. Comparing (2.21) with (2.9) and (2.10), we observe that $\mathbf{x}_A = \mathsf{H}(t) \cdot \mathbf{X}_A$ and $\mathbf{f}(\mathbf{X}_A, t) \equiv \mathsf{H}(t) \cdot \mathbf{X}_A$. Thus, the deformation and velocity gradients are

$$\mathsf{F}(t) = \mathsf{H}(t) \tag{2.51a}$$

and

$$\mathsf{L}(t) = \dot{\mathsf{H}}(t) \cdot \mathsf{H}(t)^{-1}, \tag{2.51b}$$

respectively, the same as in the previous example. Similarly, the velocity and acceleration in frame $\mathscr{O}$ of some point A are obtained by simply augmenting the corresponding expressions for homogeneous deformation with P's velocity $\mathbf{v}_P(t)$ and inertial acceleration $\mathbf{a}_P(t)$ as observed in $\mathscr{O}$. We find, respectively,

$$\mathbf{v}_A(t) = \mathsf{L} \cdot \mathbf{x}_A(t) + \mathbf{v}_P(t) \tag{2.52a}$$

and

$$\mathbf{a}_A(t) = (\dot{\mathsf{L}} + \mathsf{L}^2) \cdot \mathbf{x}_A(t) + \mathbf{a}_P(t). \tag{2.52b}$$

As before, setting $\mathsf{L} = \mathsf{D} + \mathsf{W}$, in the equations above, we obtain

$$\mathbf{v}_A(t) = (\mathsf{D} + \mathsf{W}) \cdot \mathbf{x}_A + \mathbf{v}_P \tag{2.53}$$

and

$$\mathbf{a}_A(t) = (\dot{\mathsf{D}} + \mathsf{D}^2) \cdot \mathbf{x}_A(t) + (\mathsf{D} \cdot \mathsf{W} + \mathsf{W} \cdot \mathsf{D}) \cdot \mathbf{x}_A + (\dot{\mathsf{W}} + \mathsf{W}^2) \cdot \mathbf{x}_A + \mathbf{a}_P.$$

The expression for A's acceleration closely parallels the 'five-term acceleration' formula in rigid-body mechanics; cf. (2.8). The 'five-term acceleration formula' assembles the acceleration of a point moving with respect to a rigid body from the following constituents: the acceleration with respect to a reference point of a point fixed to the rigid body and coincident with the moving point; the relative acceleration of the moving point with respect to the rotating rigid body; the Coriolis acceleration that corrects the error committed by measuring the rate of change of the relative velocity of the moving point in a rotating frame; and the acceleration of the reference point. Similarly, imagine a *rigid* body that instantaneously coincides with the homogeneously deforming body, so that there is a point B on the former overlaying the 'moving point' A. Let this rigid body whose reference point – again, say, its mass center – is at P and that rotates at an angular velocity equal to $\mathbf{w}(t)$. Employing $\mathbf{w}$, the last bracketed term above may be written as $\dot{\mathbf{w}} \times \mathbf{x}_A + \mathbf{w} \times (\mathbf{w} \times \mathbf{x}_A)$. Because at time t, $\mathbf{x}_A = \mathbf{x}_B$, this is the acceleration of B – a point on the rigid body coincident with the moving point A – with respect to P. The first bracketed term comprises the relative acceleration of A with respect to B as measured by an observer who turns with the rigid body. Finally, the second bracketed term is analogous to the Coriolis acceleration.

2.7 Stress

So far we have explored the geometry of a body's deformation, along with some simple illustrations. We turn now to estimating internal forces that accompany this deformation. The appropriate entity that estimates internal forces in a continuum is found to be the *stress tensor*; see, e.g., Spencer (1980, p. 44). The *Cauchy* stress tensor $\boldsymbol{\sigma}(\mathbf{x}(t), t)$ is defined in the current configuration.[6] In the absence of a volumetric distribution of couples, and employing angular momentum balance, $\boldsymbol{\sigma}$ may be shown to be symmetric; see Spencer (1980, Sect. 5.5). The Cauchy stress tensor is related to the applied surface forces in the current configuration of the body through

$$\mathbf{t} = \hat{\mathbf{n}} \cdot \boldsymbol{\sigma} = \boldsymbol{\sigma} \cdot \hat{\mathbf{n}}, \tag{2.54}$$

where $\mathbf{t}(\mathbf{x}(t), t)$ is the *traction*, i.e., the force per unit area acting over a surface element oriented by the unit normal $\hat{\mathbf{n}}(\mathbf{x}(t), t)$. We will refer internal and external forces, their measures, and the body's geometry to location $\mathbf{x}$ relative to the reference point P; cf. (2.9). Balancing linear momentum in an infinitesimal volume element within the body's current configuration provides the local *linear momentum balance* equation

$$\nabla \cdot \boldsymbol{\sigma} + \rho \mathbf{b} = \rho \mathbf{a}^I, \tag{2.55}$$

[6] Other stress tensor definitions depending on the choice of the body's configuration are possible; see Spencer (1980, Chap. 5).

where $\nabla = \nabla_{\mathbf{x}}$ is the gradient with respect to $\mathbf{x}$, $\mathbf{b}(\mathbf{x}(t), t)$ is the body force per unit mass, $\rho(\mathbf{x}(t), t)$ is the material density and the $\mathbf{a}^I(\mathbf{x}(t), t)$ is the acceleration of a material element in an inertial frame. Replacing for $\mathbf{a}^I$ above from (2.8b) and rewriting, we obtain linear momentum balance in the rotating frame $\mathscr{O}$:

$$\nabla \cdot \boldsymbol{\sigma} + \rho \left(\mathbf{b} - \Omega^2 \cdot \mathbf{r} - \dot{\Omega} \cdot \mathbf{r} - 2\Omega \cdot \mathbf{v} \right) = \rho \mathbf{a}. \tag{2.56}$$

In the rotating frame $\mathscr{O}$, the centripetal, angular and Coriolis' accelerations are perceived as *inertial forces* contributing to the body force. In fact, introducing

$$\mathbf{b}_{rel} = \mathbf{b} - \Omega^2 \cdot \mathbf{r} - \dot{\Omega} \cdot \mathbf{r} - 2\Omega \cdot \mathbf{v} \tag{2.57}$$

as the apparent body force observed in the rotating frame $\mathscr{O}$, we may rewrite the previous linear momentum balance succinctly as

$$\nabla \cdot \boldsymbol{\sigma} + \rho \mathbf{b}_{rel} = \rho \mathbf{a}, \tag{2.58}$$

where $\mathbf{a}$ is the acceleration of a material point observed in $\mathscr{O}$.

It is important to note that (2.58) is not enough to find the stress tensor's components. Indeed, (2.58) is a vector equation, while $\boldsymbol{\sigma}$ is a symmetric tensor with six components. Thus, the system (2.58) is underdetermined, and an infinity of solutions for these components may be found. Linear momentum balance only provides relations that must be *necessarily* satisfied by *all* continuum bodies irrespective of what material they are composed; it does not deliver a unique stress tensor. We return to this later.

2.8 Moments of the Stress Tensor

Useful information is obtained from the linear momentum balance equation by taking moments of (2.58) of appropriate order. A *moment* of order n is obtained by taking successively n tensor products of the linear momentum balance Eq. (2.58) with the relative position vector $\mathbf{x}(t) = \mathbf{r}(t) - \mathbf{r}_P(t)$, and then integrating the resulting equation over the body's current volume V. In the following, we identify P with the center of mass of the body, so that

$$\int_V \mathbf{x} \rho \mathrm{d}V \equiv 0 \quad \text{and} \quad \int_V \mathbf{r} \rho \mathrm{d}V = \mathbf{r}_P. \tag{2.59}$$

We introduce the process by obtaining the *zeroth moment* that is simply the average of (2.58):

$$\int_S \mathbf{t} \mathrm{d}S + \int_V \rho \mathbf{b}_{rel} \mathrm{d}V = \int_V \rho \mathbf{a} \mathrm{d}V = m \mathbf{a}_P, \tag{2.60}$$

which, recognizing that the left-hand side is the sum of all external and inertial forces acting on the body, simply reflects global conservation of the body's linear momentum in the rotating frame $\mathscr{O}$. Here, in the first integral on the left we employed the divergence theorem from Sect. 1.5.2 to find $\int_V \nabla \cdot \boldsymbol{\sigma}\, \mathrm{d}V = \int_S \boldsymbol{\sigma} \cdot \hat{\mathbf{n}} \mathrm{d}S$, and from (2.54) recognized $\boldsymbol{\sigma} \cdot \hat{\mathbf{n}}$ as $\mathbf{t}$, the traction on the surface. On the right side, we computed

$$\int_V \rho \mathbf{a} \mathrm{d}V = \int_V \rho \ddot{\mathbf{r}} \mathrm{d}V = \frac{\mathrm{d}^2}{\mathrm{d}t^2} \int_V \rho \mathbf{r} \mathrm{d}V = m \ddot{\mathbf{r}}_P,$$

where in the third step we utilized (2.45).

The *first moment* of (2.58) is obtained by evaluating

$$\int_V \mathbf{x} \otimes [\rho \mathbf{b}_{rel} + \nabla \cdot \boldsymbol{\sigma} = \rho \mathbf{a}]\, \mathrm{d}V,$$

where we suppress the time and space variation of various quantities. Because $\mathbf{x} \otimes \nabla \cdot \boldsymbol{\sigma} = \nabla \cdot (\mathbf{x} \otimes \boldsymbol{\sigma}) - \boldsymbol{\sigma}$, the above equation becomes

$$\int_V \mathbf{x} \otimes \rho \mathbf{b}_{rel}\, \mathrm{d}V + \int_V \nabla \cdot (\mathbf{x} \otimes \boldsymbol{\sigma}) \mathrm{d}V - \int_V \boldsymbol{\sigma}\, \mathrm{d}V = \int_V \mathbf{x} \otimes \rho \mathbf{a}\, \mathrm{d}V.$$

Again, by the divergence theorem, $\int_V \nabla \cdot (\mathbf{x} \otimes \boldsymbol{\sigma}) \mathrm{d}V = \int_S \mathbf{x} \otimes \boldsymbol{\sigma} \cdot \mathbf{n} \mathrm{d}S$, and employing (2.54), we may rewrite the previous equality as

$$\int_V \boldsymbol{\sigma}\, \mathrm{d}V = \overline{\boldsymbol{\sigma}} V = -\int_V \mathbf{x} \otimes \rho \mathbf{a}\, \mathrm{d}V + \int_V \mathbf{x} \otimes \rho \mathbf{b}_{rel}\, \mathrm{d}V + \int_S \mathbf{x} \otimes \mathbf{t}\, \mathrm{d}S, \tag{2.61}$$

where $\overline{\boldsymbol{\sigma}}$ is the average stress and V the body's current volume. In the above equation, the last term on the right is the first moment of the traction, the middle term is the first moment of the body forces, and the first term is the (first) moment of momentum.

We caution the reader against confusing the above usage of 'moment' with its identification as *torque* in rigid-body mechanics. The torque of a vector, typically the force, is the cross product of that vector with the position vector. As (1.28b) shows, the cross product may be obtained from the tensor product, so that the torque of a vector may be extracted from its first moment. For example, the total rate of change of angular momentum $\mathbf{h}_P(t)$ about the center of mass of the body is

$$\begin{aligned} \dot{\mathbf{h}}_P &= -2\, \mathrm{ax\,sk} \int_V \mathbf{x} \otimes \rho \mathbf{a}^I \mathrm{d}V \\ &= -2\, \mathrm{ax\,sk} \int_V \mathbf{x} \otimes \rho \left(\mathbf{a} + \Omega^2 \cdot \mathbf{x} + \dot{\Omega} \cdot \mathbf{x} + 2\Omega \cdot \mathbf{v} \right) \mathrm{d}V \end{aligned} \tag{2.62}$$

where the second equality follows from an application of (2.8b) and the fact that P is the body's mass center.

We note that (2.61) is also called Signorini's theorem of stress means; see Signorini (1932) and Truesdell and Toupin (1960, p. 574). Its importance lies in the fact that were $\ddot{\mathbf{x}}$ known in $\mathscr{O}$, the *average* value of the stress tensor may be found *exactly* in terms of the applied tractions $\mathbf{t}$ and the body force field $\mathbf{b}_{rel}$.

In (2.61), because the stress tensor is symmetric, the left-hand side represents only six independent variables. This indicates that the anti-symmetric part of the right-hand side of (2.61) must vanish. Imposing this requirement, we find

$$\begin{aligned} 0 &= \operatorname{ax}\operatorname{sk}\left[-\int_V \mathbf{x}\otimes\rho\mathbf{a}\,\mathrm{d}V+\int_V \mathbf{x}\otimes\rho\mathbf{b}_{rel}\,\mathrm{d}V+\int_S \mathbf{x}\otimes\mathbf{t}\,\mathrm{d}S\right] \\ &= \operatorname{ax}\operatorname{sk}\left[-\int_V \mathbf{x}\otimes\rho\left(\mathbf{a}+\Omega^2\cdot\mathbf{x}+\dot{\Omega}\cdot\mathbf{x}+2\Omega\cdot\mathbf{v}\right)\mathrm{d}V+\int_V \mathbf{x}\otimes\rho\mathbf{b}\,\mathrm{d}V+\int_S \mathbf{x}\otimes\mathbf{t}\,\mathrm{d}S\right], \end{aligned}$$

where we have employed the equivalence between an anti-symmetric tensor and its axial vector, and employed (2.8b) and (2.57) for $\mathbf{a}$ and $\mathbf{b}_{rel}$, respectively. Multiplying the above by '-2' and recognizing from (2.62) that the first term is then the rate of change of the body's angular momentum, while from (1.28b) that the remaining two terms represent the torque due to the body and surface forces, respectively, we finally arrive at

$$\dot{\mathbf{h}}_P(t)=\int_V \mathbf{x}(t)\times\rho(\mathbf{x},t)\mathbf{b}(\mathbf{x},t)\mathrm{d}V+\int_S \mathbf{x}(t)\times\mathbf{t}(\mathbf{x},t)\mathrm{d}S, \tag{2.63}$$

which is simply a statement about the global conservation of angular momentum about the mass center.

Higher-order stress moments may be generated in a manner similar to the first moment. For example, the second moment is given by

$$\int_V \mathbf{x}\otimes\mathbf{x}\otimes[\rho\mathbf{b}_{rel}+\nabla\cdot\boldsymbol{\sigma}=\rho\mathbf{a}]\,\mathrm{d}V.$$

Resolving the integral involving $\boldsymbol{\sigma}$ as

$$\int_V \mathbf{x}\otimes\mathbf{x}\otimes\nabla\cdot\boldsymbol{\sigma}\,\mathrm{d}V=\int_S \mathbf{x}\otimes\mathbf{t}\,\mathrm{d}S-\int_V(\mathbf{x}\otimes\boldsymbol{\sigma}+\boldsymbol{\sigma}\otimes\mathbf{x})\,\mathrm{d}V,$$

we obtain the second moment to be

$$\begin{aligned} \int_V(\mathbf{x}\otimes\boldsymbol{\sigma}+\boldsymbol{\sigma}\otimes\mathbf{x})\,\mathrm{d}V=&-\int_V \mathbf{x}\otimes\mathbf{x}\otimes\rho\mathbf{a}\,\mathrm{d}V+\int_V \mathbf{x}\otimes\mathbf{x}\otimes\rho\mathbf{b}_{rel}\,\mathrm{d}V \\ &+\int_S \mathbf{x}\otimes\mathbf{x}\otimes\mathbf{t}\,\mathrm{d}S. \end{aligned} \tag{2.64}$$

The equation above allows us to determine the first moment of the stress tensor, adding to our knowledge about the stress tensor's average obtained previously from the first moment (2.61). Indeed, because the second moment is in terms of third-order tensors

that are *all* symmetric in their first two components, the above tensorial equations represent 18, and *not* 27, independent equations for the 18 components of $\mathbf{x} \otimes \boldsymbol{\sigma}$. Thus, we have *just* enough equations. In contrast, in (2.61), the stress tensor on the left side had *six*, while each "load" moment tensor on the right side had *nine* independent elements. The "left-over" three equations yielded global angular momentum balance. For higher moments, the number of stress moments exceeds the number of load moments, so that all stress moments of that order *cannot* be determined. In fact, from moments of order $n \geqslant 3$, *not* all components of the $(n-1)$th-stress moment may be found. As Truesdell and Toupin (1960, p. 576) note, the reason for this lies in the fact that linear momentum balance (2.58) yields non-unique stresses. If we had obtained enough equations for every n, the stress tensor could be characterized independently of the material constituting the body, through its moments, to as great a degree as desired, simply by taking successively higher moments of (2.58).

2.9 Power Balance

The first law of thermodynamics states that the rate of change of total energy stored in a system must balance the sum of the net mechanical power delivered/extracted from the system by the environment and the rate at which any other energy enters the system. Energy may be stored and exchanged in many forms; these include mechanical motion, elastic energy, heat flux, electromagnetic currents, etc. We will here consider only the interplay between mechanical power, elastic energy and heat.

In a deformable body, energy is stored both as *kinetic energy* and *internal energy*. The kinetic energy is given by

$$E_K = \frac{1}{2} \int_V \left|\mathbf{v}^I\right|^2 \rho \mathrm{d}V, \tag{2.65}$$

obtained by summing up the kinetic energies of infinitesimal mass elements $\rho \mathrm{d}V$ over the body's volume V. The internal energy is expressed in terms of the *internal energy density* e as

$$E_I = \int_V e\rho \mathrm{d}V. \tag{2.66}$$

The internal energy density includes both the energy stored as *elastic energy* and also as heat. The exact form of the elastic energy will depend on the specific mechanical behavior of the material to be addressed in Sect. 2.10. The rate at which mechanical work is done on the body includes the power delivered to it by body and surface forces, while the heat-flux vector $\mathbf{q}$ estimates the amount of heat flowing *out* of the system. Thus, we write the total thermo-mechanical power input to the system as

$$P_{in} = \int_V \mathbf{v}^I \cdot \rho \mathbf{b} \, \mathrm{d}V + \int_S \mathbf{v}^I \cdot \mathbf{t} \mathrm{d}S - \int_S \mathbf{q} \cdot \hat{\mathbf{n}} \mathrm{d}S.$$

where $\mathbf{b}$ is the body force field per unit mass, and $\mathbf{t}$ is the traction acting on body's surface S. Balancing rate of energy change with the power delivered we obtain

$$\frac{\mathrm{d}}{\mathrm{d}t}\int_V \left(\frac{1}{2}\left|\mathbf{v}^I\right|^2 + e\right)\rho \mathrm{d}V = \int_V \mathbf{v}^I \cdot \rho\mathbf{b}\rho \mathrm{d}V + \int_S \mathbf{v}^I \cdot \mathbf{t}\,\mathrm{d}S - \int_S \mathbf{q}\cdot\hat{\mathbf{n}}\mathrm{d}S. \tag{2.67}$$

To obtain a differential form for the power balance, we first introduce (2.54) into the second integral on the right, and then employ the divergence theorem to convert both the surface integrals to volume integrals. We then invoke (2.45) to arrive at the balance

$$\int_V \frac{\mathrm{d}}{\mathrm{d}t}\left(\frac{1}{2}\left|\mathbf{v}^I\right|^2 + e\right)\rho \mathrm{d}V = \int_V \mathbf{v}^I \cdot \rho\mathbf{b}\,\mathrm{d}V + \int_V \nabla\cdot(\mathbf{v}^I\cdot\boldsymbol{\sigma})\mathrm{d}V - \int_V \nabla\cdot\mathbf{q}\,\mathrm{d}V.$$

Though in the above V is the body's volume, it is clear that the above equality holds also for arbitrary volumes within the body. Thus, we must have

$$\frac{1}{2}\rho\overset{\cdot}{\left|\mathbf{v}^I\right|^2} + \rho\dot{e} = \rho\mathbf{b}\cdot\mathbf{v}^I + \mathbf{v}^I\cdot\nabla\cdot\boldsymbol{\sigma} + \boldsymbol{\sigma} : \left(\nabla\mathbf{v}^I\right)^T - \nabla\cdot\mathbf{q},$$

where we have expanded $\nabla\cdot(\mathbf{v}^I\cdot\boldsymbol{\sigma})$. Now $\nabla\mathbf{v}^I = \tilde{\mathsf{L}}$, while from (2.4) we find that $\overset{\cdot}{\left|\mathbf{v}^I\right|^2} = \overset{\circ}{\left|\mathbf{v}^I\right|^2} = 2\mathbf{v}^I\cdot\mathbf{a}^I$. This allows us to reorganize the above equation as

$$\mathbf{v}^I\cdot\left[\rho\mathbf{a}^I - \rho\mathbf{b} - \nabla\cdot\boldsymbol{\sigma}\right] + \rho\dot{e} = \boldsymbol{\sigma} : \tilde{\mathsf{L}} - \nabla\cdot\mathbf{q}.$$

From the linear momentum balance (2.55), the bracketed term vanishes. We invoke (2.39) and (2.36) to split $\tilde{\mathsf{L}}$, and utilize (1.29e), to finally obtain

$$\rho\dot{e} = \boldsymbol{\sigma} : \mathsf{D} - \nabla\cdot\mathbf{q}. \tag{2.68}$$

This represents the balance within a infinitesimal material volume of the rate of change of the internal energy with the *stress power* $\boldsymbol{\sigma} : \mathsf{D}$ and the heat flux delivered to that material volume.

2.10 Constitutive Laws

We have noted that linear momentum balance (2.58), which is valid for all bodies, irrespective of their material composition, is insufficient to provide complete information of the stress tensor. This is expected, because, if this were not the case, then all bodies, no matter what their internal constitution, will require identical force distributions to have the same motion. Experience informs us that this is not the case. It is easier to compress/elongate rubber than steel by the same amount. Therefore

additional information is required to distinguish disparate materials. This information will be in terms of *constitutive laws* that relate stresses to measures of local deformation. Typically, these latter measures include strains and strain rates.

Some common material models include rigid bodies and inviscid fluids. In a rigid object their is no deformation, and distances between points and their relative orientations are preserved. Thus, only (2.58) provides information about the stress tensor. Because of inadequate number of equations, it is impossible to obtain a pointwise specification of the stress tensor. Locally, the stress is whatever is required to maintain rigidity. However, as demonstrated in the next chapter, the *average* stress within a rigid body may be found *exactly*. Inviscid fluids are characterized by their inability to support shear stress, statically or dynamically. Thus, only an isotropic state of pressure can be present.

We now discuss a constitutive law that we will employ to model granular materials.

2.10.1 Rigid-Perfectly Plastic Materials

It is observed that the constitutive response of materials such as metals or sands is linear and reversible (elastic) at smaller loads, but becomes nonlinear and irreversible for larger loads. This latter behavior is termed *plasticity*. Classical plasticity theory (Hill 1950, Chen and Han 1988) is concerned with developing constitutive laws that capture both the linear-elastic and plastic behaviors of a material. The major ingredients involve assuming (i) a well-defined *yield criterion* that separates linear-elastic and plastic responses, (ii) a *flow rule* to relate kinematics post-yield, (iii) a *consistency condition* that enforces that the stress state within the material continues to satisfy the yield criterion when flowing plastically, (iv) a *hardening law* that captures any changes in the yield criterion due to plastic flow, and (v) an *unloading criterion* that specifies how yielding may cease. Simplification is possible by neglecting the strains accumulated because of the material's elastic response in comparison with its plastic deformation. This prompts the study of *rigid-plastic* materials. Still further reduction is afforded by assuming that the yield criterion remains unchanged during plastic flow, so that hardening is ignored and we are led to *rigid-perfectly plastic* materials. Here, we will consider only rigid-perfectly plastic materials, but, for brevity will often label them merely as 'rigid-plastic' or even 'plastic' materials.

A rigid-plastic material remains rigid until yielding occurs as determined by some criterion being violated, beyond which plastic flow begins. Because we ultimately seek to employ this constitutive model to describe the behavior of granular aggregates, the yield criterion of choice must be characteristic of such materials. A first choice could be the *pressure criterion* that hypothesizes that yielding occurs whenever the pressure

$$p = -\frac{1}{3}\text{tr}\,\boldsymbol{\sigma} \tag{2.69}$$

ceases to be compressive (positive). This is an attempt to model the fact that, because granular materials cannot sustain tensile stresses in the absence of cohesion, a negative pressure will cause the material to cavitate. However, it may happen that the pressure can be positive even while one or two principal stresses are tensile. This suggests the improved *tensile criterion* that captures the fact that dry granular materials will yield if any principal stress is tensile. However, even when all principal stresses are compressive, the aggregate can yield if the shear stress on some plane in its interior overcomes the resistance due to particle interaction. Note that even when the grains comprising the aggregate are taken to be smooth, such as the smooth spheres employed in the simulations of Richardson et al. (2005), there will be some resistance to deformation due to interlocking of the aggregate's constituents. This interlocking is typically modeled as an internal geometric friction, i.e., a frictional resistance whose origins lie in the particles' geometry and arrangement, rather than in their surface interaction. Thus, an appropriate yield criterion governing the transition from a rigid state where the constituents are locked together, to a more mobile granular state that is in turn modeled as plastic flow, could be the *Mohr–Coulomb yield criterion*, or its smoothed version in stress space, the *Drucker–Prager criterion*. Both these criteria are stated in terms of an internal friction angle and are discussed below. Note that the tensile criterion is a particular case of these, when the internal friction angle equals 90°.

We now detail the equations governing the behavior of a rigid-perfectly plastic material. More details may be found in any book on plasticity, e.g., Chen and Han (1988). The *Mohr–Coulomb yield criterion* states that material will not yield if

$$\sigma_{max} - k_{MC}\sigma_{min} \leq 0, \tag{2.70}$$

where k_{MC} is related to the internal friction angle ϕ_F by

$$k_{MC} = \frac{1 + \sin\phi_F}{1 - \sin\phi_F} \tag{2.71}$$

and $\sigma_{max} = \max\{|\sigma_i|\}$ and $\sigma_{min} = \min\{|\sigma_i|\}$ are the extreme principal stresses known in terms of the principal stresses σ_i. Here we prefer to employ the *Drucker–Prager criterion* for both static and dynamical analyses. This preserves continuity between the two situations, and its smoothness facilitates numerical calculations. To formulate the Drucker–Prager yield criterion, we define the *deviatoric stress tensor*

$$\mathsf{s} = \boldsymbol{\sigma} + p\mathsf{1}. \tag{2.72}$$

The Drucker–Prager condition may then be written as

$$|\mathsf{s}|^2 \leq k^2 p^2, \tag{2.73}$$

where $|\mathsf{s}|$ is the magnitude of the deviatoric stress obtained from (1.23) as

$$|\mathsf{s}|^2 = s_{ij}s_{ij},$$

and

$$k = \frac{2\sqrt{6}\sin\phi_F}{3 - \sin\phi_F} \tag{2.74}$$

is defined so that the Drucker–Prager yield surface is the outer envelope of the Mohr–Coulomb yield surface obtained from (2.70); see Chen and Han (1988 p. 96, Fig. 2.28). As the friction angle lies between 0° and 90°, $0 \geqslant k \geqslant \sqrt{6}$. Finally, in terms of σ_i, $|\mathsf{s}|$ may be put into the illuminating form

$$|\mathsf{s}|^2 = \frac{1}{3}\left[(\sigma_2 - \sigma_3)^2 + (\sigma_3 - \sigma_1)^2 + (\sigma_1 - \sigma_2)^2\right] = \frac{2}{3}\left(\tau_1^2 + \tau_2^2 + \tau_3^2\right), \tag{2.75}$$

where $\tau_i = (\sigma_j - \sigma_k)/2$, $(i \neq j \neq k)$ are the principal *shear* stresses at a point, so that $|\mathsf{s}|$ may be thought of as a measure of the local shear stress. Thus, like the Mohr–Coulomb yield criterion, the Drucker–Prager yield criterion (2.73), along with (2.74), also puts a limit on the allowable local shear stresses in terms of the local pressure and the internal friction angle. This interpretation will be found useful when understanding results in later chapters. Figure 2.2 shows both the yield criteria. In each case, the material is rigid when inequality holds in either (2.70) or (2.73). However, at equality, depending on the external loading, the material may yield, or remain rigid, but precariously poised at the edge of yielding.

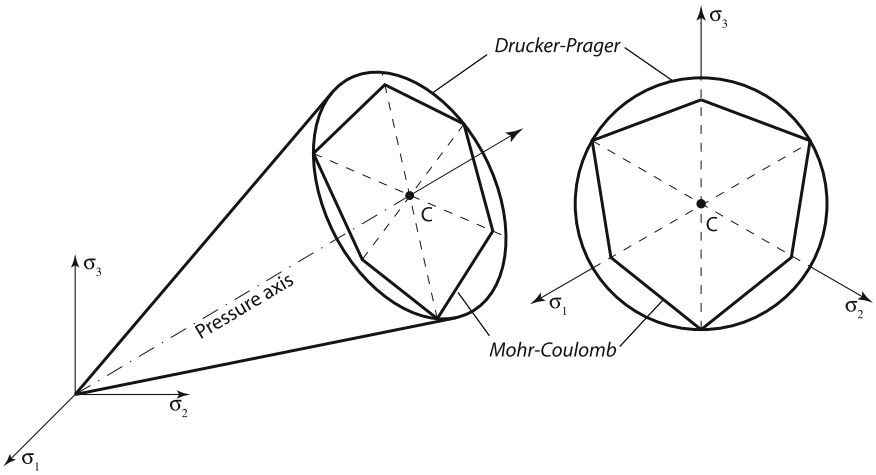

Fig. 2.2 The Drucker–Prager and the Mohr–Coulomb yield surfaces shown in the principal stress space. Both yield surfaces are centered about the pressure axis ($\sigma_1 = \sigma_2 = \sigma_3$). While the Drucker–Prager yield criterion describes a circular cone, the Mohr–Coulomb criterion defines an irregular hexagonal pyramid. The figure on the right displays both yield surfaces on a plane perpendicular to the pressure axis

With increasing loads, it may happen that a body yields at one or more places. This happens when, at any stage in a loading program, the stress state at a point violates the yield criterion. Here the stress is estimated after assuming that the regions in the body where yielding has taken place, if any, remain as they were at the previous stage of loading. Post-yielding, erstwhile rigid material will begin to flow; this is termed *plastic flow*. It will be necessary to relate this plastic flow to the stresses in the flow – the *plastic stresses*. This is traditionally accomplished by assuming a *plastic potential* g that depends only on the principal stresses. From g a *flow rule* relating the stress tensor to strain rates may be derived. The plastic potential plays a role in plasticity analogous to the *work function* in elasticity; see Fung (1965) or Holzapfel (2001). It defines a surface in stress space that allows the stresses to be related to strain increments.[7] For our purposes we employ the plastic potential

$$g = |\mathsf{s}|^2 - 9\varepsilon p^2, \tag{2.76}$$

where ε is a *dilatation parameter* lying between zero and $k^2/9$, and as we will see below, controls the extent of volume change during plastic flow. It is customary to choose the yield conditions (2.73) to define an *associative* plastic potential and, so, define an *associative flow rule*. The dilatation predicted by the associative flow rule is, however, much higher than observed values. We, therefore, choose the above form as it allows us regulate the extent of dilatation.

To obtain the flow rule, we proceed by assuming that when a body is stressed beyond yield, the incremental strain $\delta\boldsymbol{\varepsilon}$ – thought of as a six-dimensional vector – at a stress state is normal to the surface described by g passing through that stress point, i.e., $\delta\boldsymbol{\varepsilon} \propto \nabla_\sigma g$, or in indical form,

$$\delta\varepsilon_{ij} \propto \mathrm{d}g/\mathrm{d}\sigma_{ij} = s_{ij} - \frac{\varepsilon}{3}\sigma_{kk}\delta_{ij} = s_{ij} + \varepsilon p\delta_{ij},$$

where the equality follows from differentiating (2.76). For reasons to be discussed at length in Sect. 7.2.3, the above displacement $\delta\varepsilon$ is said to be *compatible* to the stress state to which it is normal; cf. point 'E' in Fig. 2.3. Introducing the proportionality parameter δc, the above can be written as

$$\delta\boldsymbol{\varepsilon} = (\mathsf{s} + \varepsilon p\mathsf{1})\,\delta c,$$

which, after converting to a rate form, becomes the flow rule

$$\mathsf{D} = (\mathsf{s} + \varepsilon p\mathsf{1})\,\dot{c}, \tag{2.77}$$

where D is the symmetric strain rate tensor and $\dot{c}$ is the *plastic multiplier*. Because we began with a plastic potential g that need not coincide with the yield surface f, the above flow rule is called *non-associative*. In the special case when g is the same

[7] In contrast, the work function in elasticity relates stress to strain, not its increment.

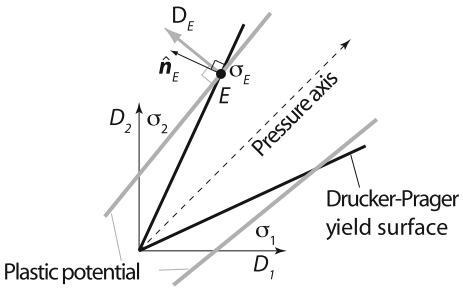

Fig. 2.3 The Drucker–Prager yield surface of Fig. 2.2 is projected onto the two-dimensional $\sigma_1 - \sigma_2$ plane. It appears as two heavy black lines bisected by the pressure axis $\sigma_1 = \sigma_2$, which is indicated by a dashed line. The stress state at yielding of a material that obeys the Drucker–Prager yield criterion lies at the point E. The unit vector $\hat{\mathbf{n}}_E$ is normal to the yield surface at E. The principal strain space is also shown. The plastic potential (2.76) provides a surface passing through E that is marked by gray lines. The strain rate D_E, thought of as a vector in principal strain-rate space, is compatible to the stress state $\boldsymbol{\sigma}_E$ if it is normal to the surface of the plastic potential at E. We may find D_E from (2.77)

as f we obtain the *associative* flow rule. To obtain $\dot{c}$, we combine (2.77) with the yield criterion (2.73) and obtain

$$\dot{c} = \frac{1}{p\sqrt{k^2 + 3\varepsilon^2}} \, |\mathsf{D}| \,, \tag{2.78}$$

with $|\mathsf{D}|^2 = D_{ij} D_{ij}$ as before. Using the above in (2.77), we obtain the plastic shear stress in terms of the strain rate:

$$\mathsf{s} = p \left(\sqrt{k^2 + 3\varepsilon^2} \frac{\mathsf{D}}{|\mathsf{D}|} - \varepsilon 1 \right), \tag{2.79}$$

where p is the pressure defined in (2.69). Combining the above with (2.72) yields the complete plastic stress tensor

$$\boldsymbol{\sigma} = -p(1+\varepsilon)1 + p\sqrt{k^2 + 3\varepsilon^2} \frac{\mathsf{D}}{|\mathsf{D}|}, \tag{2.80}$$

which, in component form, reads

$$\sigma_{ij} = -p(1+\varepsilon)\delta_{ij} + p\sqrt{k^2 + 3\varepsilon^2} \frac{D_{ij}}{\sqrt{D_{kl} D_{kl}}}.$$

Taking the trace of (2.80) and employing (2.69) we find the *dilatation rate*

$$\mathrm{tr} D = \frac{3\varepsilon \, |D|}{\sqrt{k^2 + 3\varepsilon^2}}. \tag{2.81}$$

We observe that except when $\varepsilon = 0$, the material dilates post-yield, and we need to postulate a relation between the pressure and the dilatation. A simple rate-independent linear relationship is:

$$\dot{p} = -\kappa \operatorname{tr} \mathsf{D}, \tag{2.82}$$

where κ is the *plastic bulk modulus* of the granular aggregate, i.e., bulk modulus post–yield. Because (2.81) is positive, the material expands after yielding leading to a drop in the pressure. In the special case that $\varepsilon = 0$, the flow of the material after yielding is incompressible, and the rate of change of the pressure can*not* be determined from constitutive equations. Instead, from (2.40), we obtain the additional kinematic condition expressing incompressibility:

$$\dot{\Delta} = \operatorname{tr} \mathsf{D} = 0. \tag{2.83}$$

If during plastic flow, stresses are lowered due to external conditions or structural changes introduced by large-scale yielding, the yielded regions may again become rigid. To obtain a criterion for this *unloading* from a plastic to a rigid state, we first note that during plastic flow the material's stress state remains on the yield surface, i.e., the yield function

$$f = |\mathsf{s}|^2 - k^2 p^2$$

that defines the Drucker–Prager yield surface vanishes; cf. (2.73). This may be verified by direct substitution of the stresses from (2.80) into f. Consequently, during plastic flow the incremental change

$$\delta f = 0, \quad \text{so that} \quad \dot{f} = 0.$$

This is the *consistency condition* mentioned at the beginning of this section. Simo and Hughes (1997, Sect. 2.2.2.2) and Koiter (1960, p. 173, Eq. 2.19) show that unloading takes place only when the three conditions

$$f = 0, \quad \delta f < 0 \quad \text{and} \quad \dot{c} = 0$$

are together satisfied. The first of these conditions is necessary for the material to be in a plastic state before transition. The second is a requirement that post-transition to a rigid state the stress state of the material must satisfy the yield condition (2.73) without equality. The final stipulation is equivalent to demanding that at transition the strain rate be zero. To see this, note from (2.78) that during plastic flow $\mathsf{D} \neq 0$, so that $\dot{c} > 0$. Thus, for unloading from a plastic state to possibly initiate, the strain rate $|\mathsf{D}|$ must first fall to zero. In other words, plastic flow must cease before the material may transfer to a rigid state. Until this happens, $\dot{c}$ remains positive, and plastic flow continues. It is also possible for $\dot{c}$ to vanish but δf to remain zero, so that the material persists in a plastic, albeit neutrally loaded state.

We observe that the stress tensor (2.80) depends on the strain rate through the ratio $\mathsf{D}/|\mathsf{D}|$, and so is reminiscent of dry friction with k and p essaying the role of a friction coefficient and a normal force, respectively. This should be compared with the rate-dependent constitutive relations frequently employed for rapid granular flows developed by Jenkins and Savage (1983) and Jenkins and Richman (1984, 1985). We also note that if the internal friction angle ϕ_F is set to zero, the rigid-perfectly plastic material has no shear strength and behaves as an inviscid fluid. This observation will help make contact with extensive work already available for fluids.

We will model rubble-pile *minor planets*[8] as being comprised of a rigid-perfectly-plastic material with a Drucker–Prager yield surface. For post-yield situations, the yield criterion is coupled with an appropriate flow rule to provide stresses during plastic flow, along with suitable conditions governing transition back to a rigid state. Throughout, we assume the body to be isotropic and homogenous.

We now discuss the possible values for the constitutive parameters ϕ_F and κ for the case of granular materials like soils.

2.10.2 Material Parameters

Soils display extremely complex stress response, and constitutive models such as the popular cam-clay model have very many parameters; see, e.g., Bolton (2003, p. 210). However, given that very little is known about the physical nature of minor planets, utilizing a material model with many parameters appears unwarranted. Thus, here we model the material response of dry granular aggregates as a rigid-perfectly plastic material with only two constitutive parameters, viz., the internal friction angle ϕ_F that defines the yield surface, and the plastic bulk modulus κ that describes the flow post-yield. Both these parameters depend on the manner in which the aggregate is packed and the properties of its constituent grains. For dry materials, the aggregate's packing may be described in terms of its *void ratio*[9] and the average pressure confining the aggregate. A popular and versatile method of probing soils is the *triaxial test*; see, e.g., Bolton (2003, p. 189) for a detailed description. The setup involves first confining a sack containing sand at some void ratio at an initial pressure by immersing it in a fluid. The sack is then sheared by compressing it incrementally along its axis, so that the axial and lateral directions are then the principal stress/strain directions. The internal friction angle ϕ_F is found by measuring the ratio r of the axial to the lateral principal stress at yield, and invoking the formula $\phi_F = \sin^{-1}[(r-1)/(r+1)]$. A typical response of the principal stress ratio r with axial compression during a single triaxial test is shown in Fig. 2.4. We observe from Fig. 2.4 that r goes through a maximum before settling into a lower limiting value. The maximum of r corresponds to the *peak* strength of the soil, while its limiting value is the *ultimate* strength of the soil. The soil is said to have yielded when its peak strength is reached. It then subsequently *softens*

[8] We label any substantial Solar System object, which is not a major planet as a minor planet.

[9] Ratio of the free volume in an aggregate to the volume occupied by grains.

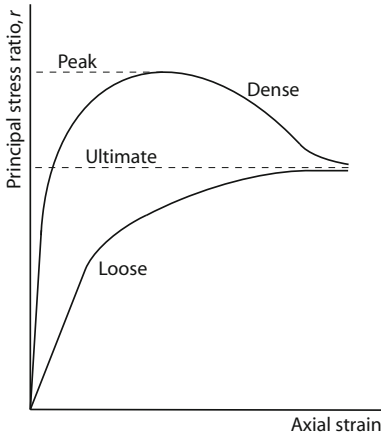

Fig. 2.4 Typical variation with axial compression of the ratio r of the axial and lateral stresses during triaxial tests of initially dense and loose soils. This figure is illustrative

to a final *critical* state. The critical state of a soil is characterized by an ultimate friction angle and a void ratio that depends only on the confining pressure and not the initial density of the soil; see, e.g., Bolton (2003, Sect. 4.4, p. 69). Initially loose soils often do not display a peak strength, and asymptotically reach their critical state; see Fig. 2.4.

The bulk modulus κ is found by the *hydrostatic compression test* that involves imposing additional hydrostatic loading on the same initial triaxial setup. It is found that the bulk modulus of a soil, and its peak and ultimate friction angle depend crucially on the confining pressure, while only the first two depend on the initial void ratio. These values can vary appreciably from one soil to another.

Here, we employ the ultimate friction angle as the internal friction angle ϕ_F that characterizes yield in our rigid-perfectly plastic material model. There are several reasons for doing so. First, as mentioned above, the peak strength of a soil depends on its initial density, but not so its ultimate strength. Dense soils display a peak strength, while loose soils do not. In contrast, every soil realizes its ultimate (critical) state. Furthermore, as the experiments cited below report, while the peak behavior varies greatly depending on the soil type, the ultimate strength changes little and remains within 30°–40°. Thus, given that we do not know much about the interiors or origins of minor planets that are our primary focus, it appears prudent to calibrate our theory against the critical state of a soil that differs less across soils, initial states and confining pressures. Second, the decrease in the frictional strength post-peak may be modeled by including softening within our material model; see, e.g., Chen and Han (1988 Sect. 3.6.3, p. 168). An application of the maximum dissipation postulate will then show that a softening rigid-plastic material is trivially locally unstable at first order; cf. Chap. 7. Thus, we are less likely to find objects at equilibria that require them to mobilize their peak frictional strength. Finally, we will in Chaps. 11 and 12 investigate the long-term dynamics of asteroids, and it is clear that this will be dictated by the ultimate friction angle.

Typically, experiments are done at confining pressures of one or more MPa and sand is found to have an ultimate friction angle ϕ_F between 30° and 40° (see, e.g., Nedderman 1992, p. 25, Table 3.1) and plastic bulk modulus κ of 1 MPa (Bolton 2003, Chap. 8). The peak friction angle for dense sands, though higher than ϕ_F is also within the same range of 30° – 40°. On the other hand, not much experimental data is available on sand confined at lower pressures. Ponce and Bell (1971) and Fukushima and Tatsuoka (1984) report triaxial tests conducted at confining pressures between, respectively, 1.4 and 241 kPa, and 2 and 400 kPa. These two tests utilized possibly the lowest confining pressures in terrestrial triaxial tests done till date. Recently, Sture et al. (1998) performed tests in space shuttle flights under low-gravity conditions at confining pressures of 0.05, 0.52 and 1.30 kPa.

Ponce and Bell (1971) reported that as the confining pressure reduced from about 35 to 1.4 kPa the ultimate internal friction angle ϕ_F increased sharply from about 30° to 44°. The corresponding value of peak friction for 'very dense' sands changed from 38.5° to 51.5°. This was attributed to reduced grain crushing during shearing at low pressures. For 'very loose' sands the peak and ultimate frictional strengths coincided, and was explained on the basis of lowered resistance to particle motion by neighboring particles. For the quartz sand that Ponce and Bell (1971) employed, the *relative density*[10] for very loose sands was 5 %, but 94 % for very dense ones; the corresponding void ratios are 0.71 and 0.48, respectively. On the other hand, the careful triaxial tests of Fukushima and Tatsuoka (1984) that were conducted at low confining pressures between 2 and 10 kPa, but on a different (Toyura) sand, concluded that the ultimate friction angle ϕ_F changed slightly from 33.5° to 35°. The peak strength of Toyura sand did increase as the initial void ratio was lowered, but remained invariant to changes in the confining pressures at a fixed void ratio. In fact, the peak friction angle in dense Toyura sand was found almost constant at about 43.5°. This latter conclusion was at variance with that of Ponce and Bell (1971), and emphasized the difference in the material response of different soils, especially at low confining pressures. Finally, working with Ottawa quartz sand, Sture et al. (1998) confirmed the trends of the terrestrial experiments of Ponce and Bell (1971). Sture et al. (1998) found that in sand with relative density 85 % the peak friction angle increased from 53.3° to 63.4° as the confining pressure fell from 1.30 to 0.05 kPa. At the same time, in 20 % less dense soils, the peak friction grew from 47.6° to 70° over the same decrease of confining pressure. The range of the ultimate friction angle ϕ_F too increased, albeit slightly, from 32° to 34° in terrestrial conditions to 35° – 37° in a micro-gravity environment.

In each of the three works cited above, as the hydrostatic compression test was not conducted, values of bulk modulus are not accessible from the reported data. Hydrostatic compression tests have been carried out at a confining pressure of 20 and 25 kPa by, respectively, Lancelot et al. (2006) and Lade et al. (2009); there appear to be no experiments at lower confining pressures. Lancelot et al. (2006) report a plastic bulk modulus κ of 100 kPa for loose Hotsun RF sand at a void ratio of 0.897.

[10] Ratio of the deviation of the void ratio from its maximum achievable value to the total possible change in the void ratio at a given confining pressure.

In contrast, Lade et al. (2009) observed a much higher κ of 100 MPa for loose Ottawa sand at a void ratio of 0.83, that increased to 200 MPa as the void ratio decreased to 0.62.

We saw above that soil properties show large variation with not only the void ratio and the confining pressure, but also depend crucially on the type of sand employed for experiments. Now, we require values of ϕ_F and κ at void fractions and confining pressures that we expect in granular minor planets. Assuming an average density of 2000 kg m^{-3} for a rubble-pile asteroid, and further assuming chondritic constituent grains with density about 3200 kg m^{-3} yields a void ratio of 0.6. A terrestrial soil at this void ratio would be labeled 'dense'. The corresponding volume fraction[11] is 0.625, close to the volume fraction 0.64 of randomly closed packed aggregate of same-sized spheres; see Jaeger and Nagel (1992). Now, rubble-piles in space are primarily held together by their own gravity, and thus often exist at extremely low confining pressures of the order of tens of Pascals. Indeed, we compute the average pressure[12] within 25143 Itokawa, to be as low as 4.3 Pa! This is three orders of magnitude lower than the confining pressure employed in the terrestrial triaxial tests reported above, and four orders lower than the pressure utilized in the hydrostatic compression tests experiments quoted above. The average pressure scales as the square of the size, but even then, the largest near-Earth asteroid Eros has an average internal pressure of a mere 17.7 kPa, still lower than the experiments of Lancelot et al. (2006). This suggests that excepting Sture et al. (1998), experimental soil data currently available cannot be employed to investigate most minor planets; more experiments on dense soils confined at pressures less than 100 Pa are needed.

The above discussion suggests that typically employed estimates of internal friction angle of 30° and post-yield bulk modulus of 1 MPa that were based on terrestrial experiments may not be sacrosanct. Friction angles as high as 50° may even be attainable. We will, in fact, in future chapters also find it interesting to consider the possibility of a lower ϕ_F of 20°. This is because dissimilar soils can respond very differently, for example, natural sandy gravel has an ultimate friction angle of about 25°. Furthermore, it is known that previously worked soil may have much lower *residual* frictional strengths of 10° – 15°; see Bolton (2003, Sect. 8.7.3, p. 55). Whether such reduction is observed at low confining pressures still needs to be tested. Finally, as particle rearrangements will require no effort in the absence of a confining pressure there will be no internal frictional resistance, and we therefore expect that there will be a regime of low-confining pressures wherein friction in a soil will be much reduced. Whether this regime exists and is relevant at internal pressures observed in asteroids needs experimental verification. Similarly, plastic bulk moduli of a few kilo-Pascals will be worth exploring. Physically, this reflects our expectation that contacts between the constituent grains in these asteroids will be lightly loaded resulting in a lowered plastic bulk modulus.

We also mention the experiments on dust aggregates by Blum and Schräpler (2004) that were done with a view to understand planet formation and comets. Unfortunately,

[11] Ratio of volume occupied by grains to total volume.

[12] This is found employing (2.69) and formulae (4.1) for the average stress within an asteroid.

the aggregates employed were typically very fluffy with volume fractions of about 0.15 increasing to maximum of about 0.34. These values are much lower than the volume fraction of 0.625 estimated above for granular minor planets.

In closing, we mention that Scheeres et al. (2010) suggests that in granular bodies with meter-sized or smaller constituent grains, cohesion arising from van der Waals interaction may play a role commensurate with internal gravity. Scheeres et al. (2010) propose that because of these cohesive interactions, the behavior of rubble piles in space may be analogous to powders in terrestrial conditions; this makes the case for performing experiments similar to those of Blum and Schräpler (2004), albeit with denser powders. Cohesive bodies are able to accommodate tensile stresses to some extent, and Holsapple (2007) finds that even a small amount of cohesion may allow small fast rotators to survive as rubble piles. There exist straightforward extensions of the rigid-plastic material model utilized here that may be employed to include cohesive effects; see, e.g., Chen and Han (1988 Sect. 2.3.4, p. 94). However, this is beyond the scope of this book.

References

R.J. Asaro, V.A. Lubarda, *Mechanics of Solids and Materials* (Cambridge University Press, Cambridge, 2006)

J. Blum, R. Schräpler, Structure and mechanical properties of high-porosity macroscopic agglomerates formed by random ballistic deposition. Phys. Rev. Lett. **93**(115503), 1–4 (2004)

M.D. Bolton, *A Guide to Soil Mechanics*, 3rd edn. (Universities Press, Hyderabad, 2003)

W.F. Chen, D.J. Han, *Plasticity for Structural Engineers* (Springer, New York, 1988)

H. Cohen, Pseudo-rigid bodies. Util. Math. **20**, 221–247 (1981)

H. Cohen, R.G. Muncaster, *The Theory of Pseudo-Rigid Bodies* (Springer, New York, 1988)

S. Fukushima, F. Tatsuoka, Strength and deformation characteristics of saturated sand at extremely low pressures. Soils Found. **24**, 30–48 (1984)

Y.C. Fung, *Foundations of Solid Mechanics* (Prentice-Hall, Englewood Cliffs, 1965)

D.T. Greenwood, *Principles of Dynamics* (Prentice-Hall, Englewood Cliffs, 1988)

M.E. Gurtin, *An Introduction to Continuum Mechanics* (Academic Press, San Diego, 1981)

R. Hill, *Mathematical Theory of Plasticity* (Oxford University Press, Oxford, 1950)

K.A. Holsapple, Spin limits of solar system bodies: from the small fast-rotators to 2003 EL61. Icarus **187**, 500–509 (2007)

G.A. Holzapfel, *Nonlinear Solid Mechanics* (Wiley, New York, 2001)

H.M. Jaeger, S.R. Nagel, The physics of the granular state. Science **255**, 1523–1531 (1992)

J.T. Jenkins, M.W. Richman, Grad's 13-moment system for a dense gas of inelastic spheres. Arch. Ration. Mech. Anal. **87**, 355–377 (1984)

J.T. Jenkins, M.W. Richman, Kinetic theory for plane flows of a dense gas of identical, rough, inelastic circular disks. Phys. Fluids **12**, 3485–3494 (1985)

J.T. Jenkins, S.B. Savage, Theory for the rapid flow of identical, smooth, nearly elastic spherical particles. J. Fluid Mech. **130**, 187–202 (1983)

W.T. Koiter, General theorems for elastic-plastic solids, in *Progress in Solid Mechanics*, vol. 1, ed. by I.N. Sneddon, R. Hill (North-Holland, Amsterdam, 1960), pp. 167–221

P.V. Lade, J.A. Yamamuro, C.D. Liggio Jr., Effects of fines content on void ratio, compressibility, and static liquefaction of silty sand. Geomech. Eng. **1**, 1–15 (2009)

L. Lancelot, I. Shahrour, M.A. Mahmoud, Failure and dilatancy properties of sand at relatively low stresses. J. Eng. Mech. ASCE **132**, 1396–1399 (2006)

R.M. Nedderman, *Statics and Kinematics of Granular Materials* (Cambridge University Press, Cambridge, 1992)
V.M. Ponce, J.M. Bell, Shear strength of sand at extremely low pressures. J. Geotech. Eng. ASCE (J. Soil Mech. Found. Div. ASCE), **97**, 625–638 (1971)
D.C. Richardson, P. Elankumaran, R.E. Sanderson, Numerical experiments with rubble piles: equilibrium shapes and spins. Icarus **173**, 349–361 (2005)
D.J. Scheeres, C.M. Hartzell, P. Sanchez, M. Swift, Scaling forces to asteroid surfaces: the role of cohesion. Icarus **210**, 968–984 (2010)
A. Signorini, Alcune proprietà di media nella elastostatica ordinaria. Rend. Lincei **15**, 151–156 (1932)
J.C. Simo, T.J.R. Hughes, *Computational Inelasticity* (Springer, New York, 1997)
J.J. Slawianowski, Analytical mechanics of finite homogeneous strains. Arch. Mech. **26**, 569–587 (1974)
J.J. Slawianowski, Newtonian dynamics of homogeneous strains. Arch. Mech. **27**, 93–102 (1975)
A.J.M. Spencer, *Continuum Mechanics* (Dover, New York, 1980)
S. Sture, S.N. Batiste, K.A. AlShibli, R.A. Swanson, Mechanics of granular materials at low effective pressures. J. Aerosp. Eng. ASCE **11**, 67–72 (1998)
C. Truesdell, R.A. Toupin, The classical field theories, in *Encyclopedia of Physics Vol. III/I: Principles of Classical Mechanics and Field Theory*, ed. by S. Flüugge (Springer, Berlin, 1960), pp. 226–793

http://www.springer.com/978-3-319-40489-9

Shapes and Dynamics of Granular Minor Planets
The Dynamics of Deformable Bodies Applied to Granular Objects in the Solar System
Sharma, I.
2017, XX, 354 p. 116 illus., 25 illus. in color., Hardcover
ISBN: 978-3-319-40489-9